Settling and Rheology of Suspensions of Narrow-Sized Coal Particles

Raffi M. Turian, Feng-Lung Hsu, Kostas S. Avramidis, Dong-Jin Sung, and Robert K. Allendorfer
Dept. of Chemical Engineering, University of Illinois at Chicago, Chicago, IL 60680

Settling rates, yield stresses, and shear-stress/shear-rate dependences were determined as functions of solids concentration for suspensions in water of coal particles of narrow size fractions. Particles and suspensions are characterized by coal analyses, determination of heating value, solid heat capacity and thermal conductivity, particle size analyses, and determination of densities and maximum packing concentrations for each particle size range. Analysis of the settling rate data establishes that the usually strong retardation of (hindered) settling due to concentration is compounded by particle shape effects. In addition, observed particle shapes are subsumed within particle shape classes inferred from the settling data. Shear-stress/shear-rate data for concentrated suspensions of the three larger and relatively narrower sized particles over the broad range of shear rates from about 1 to $10^4 s^{-1}$ suggest the behavior to be essentially Newtonian, albeit with a marked particle concentration augmentation. Suspensions of the smallest coal particles of broader size distribution were strongly non-Newtonian, possessing a yield stress at low shear, essentially power-law shear-thinning behavior over the intermediate range and approaching high-shear Newtonian limiting behavior above about $10^3 s^{-1}$. Relations developed include viscosity- and yield stress-concentration correlations incorporating the maximum packing volume fraction of solids. These are useful generally for suspensions and particularly as the basis for guiding the formulation of coal-water fuels.

Introduction

Highly loaded coal-water mixtures (CWM) are of interest in part because of their promise as coal-based fuels possessing liquid-fuel attributes. In addition, a lot of wet pulverized coal is produced in coal preparation processes, and it must be stored, handled, and/or transported to be further processed (for example, dewatered or pelletized) before ultimate use. Such beneficiation is necessary because undesirable constituents in coal, such as ash and especially pyritic sulfur, are usually disseminated as inclusions of varying sizes throughout the coal matrix. Effective removal of such materials requires: first, reduction of the coal down to particle sizes small enough to result in liberation of these inclusions; their separation from the mixture using one or a number of wet processes; and then washing, flotation, their combination or variants. Indeed, deep cleaning of coal requires reduction of size to very fine levels. There are, therefore, good reasons for seeking an understanding of the behavior of CWM.

This article reports on the behavior of concentrated CWM made up from narrow particle size fractions of coal obtained by sieving. Particle size is one of the primary, determinative variables defining suspension microstructure, and thus suspension stability and rheological behavior. It is known, at least for spherical particles, that particle packing is enhanced when the particle size mix is broad and that more efficient particle packing not only permits higher solids loadings but may under appropriate circumstances improve stability and rheological behavior. However, enhancement in behavior of CWM made from coal consisting of appropriate mixtures of sizes, if any, must ultimately be measured against that of CWM made from particles of narrow size. The present work, therefore, represents part of a coherent study on the effect of coal particle size on CWM properties and behavior, and, indeed, belongs to a broader, systematic program of research concerned with the properties and the behavior of particulate coals and coal

Correspondence concerning this article should be addressed to R. M. Turian.
Present addresses of: F.-L. Hsu, Lever Bros., Edgewater, NJ 07020; K. S. Avramidis, Dow Chemical U.S.A., Midland, MI 48674; and R. K. Allendorfer, Amoco Oil Co., Whiting, IN 46394.

slurries, and with their modification and control.

In this study, pulverized Pittsburgh Seam no. 8 coal was separated by sieving into four size fractions belonging to the following mesh ranges: $-120+170$, $-170+230$, $-230+325$, and -325. The number-volume or mass-mean diameters for these particles, determined using the Elzone counter, were 105.0, 76.3, 52.7 and 22.2 μm, respectively. All slurries were made up using distilled water, and all experiments were conducted at 25°C. Gravity settling experiments were carried out in 500-mL graduated cylinders in a temperature bath, yield stresses were measured directly using the vane method, and shear stress-shear rate dependences were determined using a thermostated high-pressure capillary-tube rheometer, capable of providing data over a very broad range of shear rates and tube diameters and lengths. The latter rheological determinations are particularly tedious in the case of CWM, because unlike virtually most of the large volume of published work on coal slurry rheology, our experiments embody elaborate steps aimed at scrupulous accounting for possible wall-slip and/or end effects, and they cover an unusually broad range of shear rates. Wall-slip effects, more often than not, are present with coal slurries.

In the gravity sedimentation studies, the rate of descent of the solid-liquid interface was found to be uniform for all concentrations for the three coarser and narrower particle size fractions over virtually the entire duration of the experiments, with an abrupt change of slope signifying completion of settling. These slurries formed compact, essentially incompressible, final sediments having solid volume concentrations of within about 2% of those corresponding to maximum packing determined from centrifugal sedimentation measurements. In addition, it was found that the usually strong retardation of settling arising from enhanced interparticle interactions in such concentrated suspensions was further augmented by, among other effects, particle shape effects. By contrast, the rates of descent of the solid-liquid interfaces for the slurries made of the finest particle size coal were observed to diminish as settling progressed, and the approach to final sediment formation was gradual, suggesting that for this particle size the settled solids formed a looser, compressible structure that collapsed gradually under the buoyed weight of solids from the superior layers of the sediment. These conclusions are reaffirmed by the finding that for this finest particle size the volume concentrations of solids within the final sediments resulting from gravity settling were lower than the maximum packing value from centrifugation by from about 12 to 33%.

The shear stress-shear rate dependences from the capillary rheometer, corrected for possible wall-slip and for end effects, and covering the range of shear rates from between 1 to 10^4 s^{-1}, were found to be nearly Newtonian for all slurries made up using the three larger, narrower sized, particles, and strongly non-Newtonian for all slurries made up from the smallest, broader sized, particle coal. For the Newtonian slurries, the presence of solids, at loadings approaching levels relevant to coal-water fuel (CWF) applications and therefore of interest to this work were found to lead to rather significant viscosity increases, of from about more than one to over two orders of magnitude relative to the reference liquid viscosity. The Newtonian viscosity dependences on concentration were found to follow approximately simple, single-constant relationships, incorporating the maximum packing volume fraction as a parameter. For concentrated CWM containing the finest particles, the shear stress-shear rate dependence consisted of a yield stress in the limit of vanishing shear, power-law shear-thinning behavior over the intermediate region and an approach to high-shear limiting Newtonian behavior above about 10^3 s^{-1}. This limiting infinite-shear Newtonian viscosity was found to follow a concentration dependence similar to that for the Newtonian slurries containing the larger particle sizes. Likewise, its value ranged from about 20- to about 130-fold the reference suspending liquid viscosity over the concentrated range investigated in this work. The yield stress values measured by the vane method were correlated with solid concentrations using two-parameter relationships incorporating the maximum packing volume fraction. Such relationships have been previously proposed by Avramidis and Turian (1991) and found to apply widely to different slurry systems.

Previous Work and Background Information

The range of industrially important solid-liquid mixtures is broad. As two-phase systems they are generally inherently unstable. At one end, slurries consisting of mainly coarse, dense particles will tend to separate under the influence of gravity unless there is sufficient continuous agitation or turbulent motion to sustain suspension. Such coarse particle slurries predominate, for example, in coal slurry pipeline transportation, as they do in slurry pipeline applications generally, where high concentrations of fines are not tolerated as they lead to significant pressure loss increases for the same solids loading and to increased grinding costs. They are also messy and difficult to recover. Although a fraction of fines is usually admitted in the particle mix to retard settling, the rheological approach, which strictly presumes the material to be a continuum, is of limited efficacy.

For pipeline flow of such coarse, dense slurries we have developed a hydrodynamic, multiphase flow model based on the application of conservation of mass and momentum to the individual solid components and to the continuous phase, and embodying liquid-particle, particle-particle and particle-boundary interactions (Hsu et al., 1989). It works very well; calculated results using the model and experimental data on pressure gradient as well as on detailed concentration and velocity profiles for the flows of gypsum, coal, crushed glass, sand and gravel slurries, covering a solid particle size range from 38.3 μm to 13,000 μm, and pipe diameters from 4.0 cm to 49.5 cm were found to be in excellent agreement. At the other end, mixtures consisting of very small particles, on the order of 1 μm or smaller, are colloidal, meaning that their behavior is determined largely by electrical double-layer surface interactions which clearly assume an increasingly significant role in consequence of the increase in the interface area separating the phases. The stability and rheology of such colloidal dispersions are sensitive to shear and to chemistry. The mixtures in the present work occupy a position between these two extremes; they consist of particles fine enough to permit rheological determination under appropriate constraints, but large enough to preclude a determinative role for double-layer interactions.

Particle size and size averaging

There is a tradition of classifying suspension systems in terms

Table 1. Effective Particle Diameters and Particle Size Average

Effective Particle Diameters			
d_V = vol. dia.	dia. of sphere with same volume as particle	$d_V = (6V/\pi)^{1/3}$	
d_S = surface dia.	dia. of sphere with same surface as particle	$d_S = (S/\pi)^{1/2}$	
d_{SV} = surface-vol. dia.	dia. of sphere with same external surface to vol. ratio as particle	$d_{SV} = 6(V/S) = d_V^2/d_S^2$	
d_D = drag dia.	dia. of sphere with same resistance to motion as particle in the same fluid		
d_f = free-falling	dia. of sphere with same density and free-falling velocity as particle in the same fluid		
d_{St} = Stokes diameter	free-falling dia. of particle in Stokes law region ($Re<0.2$)	$d_{St} = \sqrt{\frac{18\mu v_\infty}{(\rho_s-\rho)g}}$	
Particle Size Averages			
$\overline{d_-^m} = \Sigma n_i d_i^m/\Sigma n_i$			
$\overline{d}$ = number-length mean dia.			
$(\overline{d^2})^{1/2}$ = number-surface mean dia.			
$(\overline{d^3})^{1/3}$ = number-volume mean dia.			
$d_{WM} = \overline{d^4}/\overline{d^3}$ = weight-moment mean dia.			
n_i = number of particles of dia. d_i			

of particle size and concentration. Clearly, particle size determines to a large, though not exclusive, degree the nature and the relative significance of the forces governing suspension stability and rheology, while concentration determines the level of interparticle interaction. Industrially important suspension systems often contain particles of mixed sizes, which may have complex shapes and which may possess additional complicating attributes such as porosity, deformability and swelling. An irregularly shaped particle has no unique dimension, and the precise role of particle size as a variable, while it may be significant, is often ambiguous. For such particles, size must be expressed as a derived linear dimension determined by measuring a suitable size-dependent property of the particle, which would be presumed relevant to the particular application. The most widely used, derived particle size is the equivalent spherical diameter, that is, the diameter of a sphere which is equivalent to the particle with regard to some prescribed property. For example, the volume-diameter, d_V, or the surface-diameter, d_S, is the diameter of a sphere that has the same volume or the same surface as the particle, respectively. Various equivalent diameters are given in Table 1 (Allen, 1975). In this table, the Stokes diameter, d_{St}, is defined as the diameter of a sphere having the same density, ρ_s, and the same free-falling velocity, v_∞, as the particle falling in a fluid of the same density, ρ, and viscosity, μ, in the Stokes flow region, with $Re = (d_{St}v_\infty\rho/\mu) < 0.2$. For a spherical particle with diameter d_{St} falling in Stokes flow the drag force is given by:

$$F_D = 3\pi d_{St}\mu v_\infty = (\pi/6)d_{St}^3 g(\rho_s-\rho) \tag{1}$$

in which the second equality is the expression of the net force between gravity and buoyancy. Equation 1 gives:

$$d_{St} = [18\mu v_\infty/(\rho_s-\rho)g]^{1/2} \tag{2}$$

By definition Eq. 2 gives the Stokes diameter of the particle, and on rearrangement also the Stokes velocity v_∞. Relationships among some of the various equivalent diameters can be established. For example, for a particle with an equivalent drag diameter d_D and volume diameter d_V, falling in Stokes Law region, the equality between drag and net gravitational force is given by:

$$3\pi d_D\mu v_\infty = (\pi/6)d_V^3 g(\rho_s-\rho) \tag{3}$$

Combining Eqs. 2 and 3 we get:

$$d_{St} = (d_V^3/d_D)^{1/2} \tag{4}$$

Equation 4 is useful because the drag diameter is difficult to measure. Experimental measurements by Pettyjohn and Christiansen (1948), using isometric nonspherical particles, yield the following approximate relationship:

$$(d_{St}^2/d_V^2) \approx \sqrt{\psi} \quad \text{for } \psi > 0.67 \tag{5}$$

in which the sphericity, ψ, is defined as the ratio of the surface area of a sphere with the same volume as the particle to the surface area of the particle:

$$\psi = (d_V/d_S)^2 \tag{6}$$

Accordingly, Eqs. 4–6 give $d_D \approx d_S$, whose approximation is subject to the limitations governing Eq. 5 for particles with $\psi > 0.67$, falling in the Stokes flow regime. The approximation in Eq. 5 may be used as a qualitative measure on the departure of the particle from spherical shape for which $\psi = 1$.

In most industrially important applications solid particles consist of mixtures of sizes, often having broad size distributions. This usually makes it necessary to establish some appropriate size-averaging scheme, which, it would be hoped, provides a mean particle size representing the aggregate effect of the sizes of all the particles on the suspension property considered. There are many types of mean particle sizes, depending on the weighting function used in the averaging process, as shown in Table 1. Also, different particle size distributions can result in the same mean value. Accordingly,

the question of which sort of average size is representative (indeed, if an average value can be representative and sufficient at all) in any given situation is often unresolved. One of the aims of the present work has been to probe this problem within a context relevant to slurry properties and behavior, as will be described later. The general averaging formula for $\overline{d^m}$ given in Table 1 provides the number-weighted mean of the mth moment of the size distribution. To establish the corresponding relationships based on mass weighting, we assume that the mass, w_i, and the number, n_i, of particles having equivalent diameter d_i are related by:

$$w_i = n_i \alpha_v \rho_s d_i^3 \qquad (\alpha_v = \pi/6 \text{ for spherical particles}) \tag{7}$$

where α_v is the particle volume coefficient which, like the particle density ρ_s, is assumed to be the same for all particles in the mix. Accordingly, the mass-mean diameter is the same as the weight-moment mean diameter ($\overline{d^4}/\overline{d^3}$) given in Table 1. A significant measure of the spread of the distribution or particle dispersion is the standard deviation σ defined by:

$$\sigma_N = \{\Sigma n_i (d_i - \bar{d})^2 / \Sigma n_i\}^{1/2} = \{\overline{d^2} - \bar{d}^2\}^{1/2} \tag{8}$$

$$\sigma_M = \{\Sigma w_i (d_i - \bar{d})^2 / \Sigma w_i\}^{1/2} = \{(\overline{d^5}/\overline{d^3}) - (\overline{d^4}/\overline{d^3})^2\}^{1/2} \tag{9}$$

Settling in single-particle systems

Settling of particles in single- and multiparticle systems form the basis of important industrial solid-liquid unit operations. Such flows are complex, and as such, they lead to rather substantive mathematical problems. Theoretical studies of flows past a sphere abound and represent various departures from Stokes's classical solution of 1851 of the Navier-Stokes equations with inertia terms set equal to zero. Analytical extensions of Stokes result to nonzero, though still very small, Reynolds numbers are associated with Oseen (1910), Proudman and Pearson (1957), and Chester and Breach (1969). Oseen's analysis leads to the correction of Stokes drag force:

$$F_D = 3\pi d \mu v_\infty \{1 + (3/16)Re + O(Re^2)\} \tag{10}$$

in which the Reynolds number is defined as $Re = (d\rho v_\infty/\mu)$. Drag force prediction based on Eq. 10, on Proudman and Pearson's result which gives part of the $O(Re^2)$ correction, or on Chester and Breach's analysis which completes the $O(Re^2)$ term and provides a glimpse of the $O(Re^3)$ correction, result in modest, if any, improvement over that provided by the Stokes result. Nonetheless, Oseen's analysis in 1910, like Stokes's, deserves special standing as a major milestone in our understanding of the mathematical structure of slow flows past submerged objects. This is because it resolved and provided the mathematical remedy for one of the persistent puzzles in fluid mechanics: the hitherto irreconcilable conflict between the experimentally confirmed validity of Stokes approximation on the one hand, and the discovery of its seeming inappropriateness as the basis in iterative schemes aimed at establishing improved approximations on the other (Whitehead's Paradox[9]). Theoretical treatments of the slow fall of a sphere in the presence of boundaries include Faxen's (1922–23) and Haberman's (1956) results for the retardation of the fall velocity due to the presence of cylindrical walls, and Happel and Brenner's (1965) and Greenstein and Happel's (1968) analyses of the problem of spheres located at arbitrary positions within the cylinder, which give rise to a torque. Empirical correction formulas for cylindrical boundary effects have been developed by Lee (1947), McPherson (1947), Engez (1948), McNown et al. (1948), McNown and Newlin (1951), and Fidleris (1958). The empirical expression of Richardson and Zaki (1954), given by

$$\log_{10}(v_\infty/v_t) = d/D \tag{11}$$

was found by Garside and Al-Dibouni (1977) to give satisfactory results over a broad range of Reynolds numbers. For arbitrary Reynolds numbers, one may use the drag coefficient-Reynolds number, $C_D(Re)$, curve for spheres, and for nonspherical shapes (McCabe et al., 1985), if available. Particle shape effects on settling velocities of ellipsoidal particles at low Reynolds numbers have been calculated by McNown and Malaika (1950) by evaluating integrals in Oberbeck's theoretical solution for creeping flow past an ellipsoid of semi-axes a, b, c. The resulting modification of Stokes drag force is given by:

$$F = (3\pi d_V \mu v_\infty) K \tag{12}$$

in which the shape factor $K = d_D/d_V$ is the ratio of the Stokes settling velocity, $v_{\infty S}$, of the volume-equivalent sphere, that is, of diameter $d_V = 2(abc)^{1/3}$, to the settling velocity, v_∞, of the particle. McNown and Malaika present the values of this shape factor as plots of K against $(a/\sqrt{bc})$ for various values of (a/b), a valuable form of information on shape effects since the ellipsoid is infinitely variable from disk-like through spherical to rod-like shapes. An interesting finding in this plot is the occurrence of a geometrical region, albeit a small one, for which K is less than unity, signifying the existence of streamlined shapes which experience lower resistance than the sphere under creeping flow conditions. McNown and Malaika also present experimental data of $K = (v_{\infty S}/v_\infty)$ against particle Reynolds number, $Re = (d_V \rho v_\infty/\mu)$, for spheroidal, cylindrical prismatic and conical particles. Pettyjohn and Christiansen (1948) determined the free-settling rates for the following shapes and sphericities (ψ): sphere (1), cube octahedron (0.906), octahedron (0.846), cube (0.806), and tetrahedron (0.670). Their results suggest that the shape factor k modifying Stokes velocity ($Re \leq 0.05$) can be approximated by:

$$k = (d_{St}^2/d_V^2) = 0.843 \log(\psi/0.065) \tag{13}$$

We note that the shape factors in Eqs. 12 and 13 are related by $k = 1/K$. Experimental values of the shape factor k ranged from 0.846 for a tetrahedron to 0.972 for a cube-octahedron. Results on nonisometric particles have also been published. They include the experimental measurements of: Heiss and Coull (1952) using cylinders and rectangular parallelepipeds; Becker (1959) using prisms and cylinders; Christiansen and Barker (1965) using cylinders, prisms and disks; Isaacs and Thodos (1967) using cylinders; and Hottovy and Sylvester (1979) using roundish irregular particles. As expected, these studies confirm the fact that the particle shape has a primary effect on the settling rate.

Settling in concentrated suspensions

Settling rates in multiparticle systems are influenced by particle interaction effects, which consist of collisions among particles and hydrodynamic and nonhydrodynamic interactions. In batch settling experiments, the rate of descent of the suspension-supernatant interface during constant-rate sedimentation is determined, which corresponds to the rate of settling, U_C, of the coal particles. As the particles settle, they are displaced by an equal volume of liquid that rises with a velocity, U_W. For a slurry with volume fraction of solids ϕ continuity requires that:

$$\phi U_C + (1-\phi)U_W = 0 \tag{14}$$

Equation 14 can be used to calculate the slip velocity, $U = U_C - U_W$, which is the relative velocity between the coal and the water, and is the pertinent settling velocity. Thus, we get:

$$U = U_C - U_W = U_C/(1-\phi) \tag{15}$$

For sedimentation (as well as in fluidization where U_C in Eq. 15 is replaced by the superficial velocity U_0) dimensional analysis suggests that:

$$(U/v_t) = f[(1-\phi),\ Re_t] \tag{16}$$

where v_t is the terminal velocity of the single particle settling alone in the same fluid and container as the sedimenting suspension of uniform spheres, and $Re_t = (d\rho v_t/\mu)$ is the particle Reynolds number. The presence of container walls at a finite distance exerts a retarding effect on the falling velocity, but most workers in the past have used the terminal velocity corrected for the wall effect, v_∞. However, Garside and Al-Dibouni (1977) who examined the sedimentation problem exhaustively, and Selim et al. (1983) who re-examined this problem and also investigated the settling of multisized particle mixtures in Newtonian fluids, have found that the use of v_t gives measurably better correlation. There are many correlations in the literature for predicting the sedimentation or fluidization velocities in nonflocculating solid-liquid suspensions. For particles of uniform size, Garside and Al-Dibouni compared the predictive effectiveness of available correlations using an extensive body of experimental data. The correlations proposed by Richardson and Zaki (1954), Barnea and Mizrahi (1974), and Garside and Al-Dibouni (1977) were found to be the most reliable. Richardson and Zaki's correlation is given by the simple expression:

$$U = v_t(1-\phi)^n \tag{17}$$

with n given as a function of particle to cylinder diameter ratio, d/D, and particle Reynolds number, Re_t, by:

$$n = 4.65 + 19.5(d/D) \qquad Re_t < 0.2 \tag{18}$$

$$n = 4.36 + 17.6(d/D)Re_t^{-0.03} \qquad 0.2 < Re_t < 1 \tag{19}$$

$$n = 4.45Re_t^{-0.1} \qquad 1 < Re_t < 500 \tag{20}$$

$$n = 2.39 \qquad 500 < Re_t < 7{,}000 \tag{21}$$

According to Garside and Al-Dibouni (1977), the expression for the exponent n given by:

$$[(5.1-n)/(n-2.7)] = 0.1Re^{0.9} \tag{22}$$

yields better prediction of settling rates. For Reynolds numbers in the Stokes flow regime and negligible wall effects, Eq. 18 gives $n = 4.65$ for spherical particles, which clearly signifies a very strong concentration effect. Chong et al. (1979) have found n to be about 4.8 for spheres, 5.4 for cubic shapes, and 5.8 for brick-like and angular particles, which suggests that particle interaction effects are compounded as the shape departs from spherical geometry, resulting in further retardation of settling rate. When the terminal velocity, v_∞, of the single sphere is estimated using the drag coefficient-Reynolds number curve, Garside and Al-Dibouni recommend the following wall-effect correlations for calculating v_t for insertion in Eq. 17:

$$\frac{v_\infty}{v_t} = \left[\frac{1-0.475(d/D)}{1-(d/D)}\right]^4 \qquad Re < 0.2 \tag{23}$$

$$\frac{v_\infty}{v_t} = 1 + 2.35(d/D) \qquad 0.2 < Re < 10^3 \tag{24}$$

$$\frac{v_\infty}{v_t} = 1/[1-(d/D)^{3/2}] \qquad 10^3 < Re < 3\times 10^3 \tag{25}$$

There is an alternative scheme to that of increasing the value of the exponent n to account for the nonspherical particle shape in settling. It involves maintaining the exponent $n = 4.68$ for spheres but replacing the solid concentration ϕ in Eq. 17 by an effective value, $\kappa\phi$, which accounts in aggregate for the envelope of fluid entrained by the settling particles. The value of $\kappa(\geq 1)$ should be higher, the more complex the particle shape in consequence of the presumed larger amount of what some (for example, Steinour, 1944) have referred to as the "sphere-completing" volume of liquid associated with the particle. We note that this idea has been used, for example, by Michaels and Bolger (1962), in analyzing sedimentation in flocculating dispersions, where the effective volume is presumed to represent particle aggregates and the entrapped fluid in the interstitial space within them.

When particles of mixed sizes settle, interparticle interactions are further compounded as the faster-settling, larger particles approach and overtake the slower, smaller particles, leaving them in their wake of trailing displaced fluid. The disparities in settling velocities lead to segregation of particles by size, with the appearance of distinct sedimenting zones signifying complete segregation when the ratio of two closest sizes exceeds 1.6. Partial segregation without distinct zone formation has been observed at particle size ratios as low as 1.19. Selim et al. (1983) have investigated the sedimentation of multisized particles in concentrated suspensions and have developed a model capable of predicting sedimentation in suspensions consisting of both discrete particle size mixtures and also continuous size distributions.

Rheology of concentrated suspensions

The rheological characteristics of suspensions range over the full span of known non-Newtonian behavior, depending on the nature of the suspended solids, the suspending liquids, and the sorts of interactions prevailing between them. Suspensions in which the suspending liquid in Newtonian exhibit non-Newtonian behavior at concentrations that depend on size, size distribution, shape and deformability of the solid particles. Non-Newtonian effects are important at low concentrations for suspensions of rigid nonspherical or deformable elastic spherical particles. For suspensions of rigid spherical particles in Newtonian liquids, non-Newtonian behavior becomes important at higher concentrations as interparticle interactions become stronger. For suspensions in non-Newtonian suspending media, the presence of solids enhances nonlinear behavior. Elongated particles or particles with large aspect ratios give rise to anisotropic behavior as a preferred particle orientation is enforced under the action of the prevailing shear field.

Dispersions of particles in the colloidal range are important industrially and abound in nature. Colloidal particles may range from approximately 10^{-3} μm to the order of 1 μm, which spans approximately the range between the limits of resolution of the electron and optical microscopes. The essential distinction of colloidal dispersions resides in the very large interface separating the phases. As a result their behavior, stability and rheology are affected strongly by nonhydrodynamic, electrical double-layer forces and the way these forces accommodate the prevailing chemistry and state of shear. The stability of such dispersions is linked to the state of aggregation of the particles; their rheology is chemistry- and shear-sensitive. Our suspensions are not markedly colloidal. The observed rheological behavior of colloidal and noncolloidal suspensions may include time-independent as well as time-dependent non-Newtonian behavior.

Qualitatively, for time-independent suspensions the plot of viscosity against shear rate would have the following characteristics. At low concentrations it may be Newtonian with a concentration-enhanced viscosity, becoming mildly (usually shear-thinning) non-Newtonian at intermediate concentrations with perhaps the attainment of low- and high-shear Newtonian limiting values within the shear rate range examined and/or with the appearance of a yield value as the shear rate becomes small. As concentration increases, it will become progressively more strongly non-Newtonian with a steeply increasing viscosity with decreasing shear rate, signifying the possible appearance of a yield stress, with normally shear-thinning behavior over the intermediate shear rate range and with the attainment of either a high-shear Newtonian limiting value of the appearance of a minimum as the shear rate increases followed by an increase in viscosity, which would signify development of shear-thickening behavior at very high shear rates. The appearance of shear-thickening behavior suggests the development of high-shear-induced structure, which would have significant implications in some important operations involving CWF, such as flows through nozzles and atomization equipment.

Effective viscosity of suspensions

For Newtonian suspensions, effective or relative viscosity expressions have been proposed representing, in the main, empirical extensions of Einstein's classical result:

$$\eta_r = \eta/\eta_s = 1 + 2.5\phi \tag{26}$$

in which η and η_r are the effective and the relative viscosity of the suspension, respectively, and η_s is the viscosity of the suspending liquid. Einstein's expression is restricted to Stokes flow of suspensions of rigid, neutrally-buoyant spheres, suspended in an incompressible Newtonian liquid in such low concentrations as to preclude any interparticle interactions, and is further restricted to inclusion of only hydrodynamic forces. These restrictions are stringent. They foreclose possibilities for predicting important phenomena that have been observed in suspension rheology. Many of the expressions, which have been proposed as generalizations of Eq. 26, can be subsumed under the functional form:

$$\eta_r = \eta_r(\phi) \tag{27}$$

Table 2 lists a few relative viscosity correlations of the form of Eq. 27. This listing represents but a mere fraction of the vast number that have appeared in the literature; Rutgers (1962a,b, 1963) quotes some 97 such correlations in his review of the subject. Detailed reviews concerned with suspension viscosity, such as those by Rutgers, Thomas (1965), Jinescu (1974), and Jeffrey and Acrivos (1976) have established the limitations of the form of Eq. 27 and have exposed the inadequacies of a lot of published suspension viscosity data. Published suspension viscosity data are often of dubious value

Table 2. Relative Viscosity Relationships for Suspensions of Spheres

Author	$\eta_r(\phi)$	Remarks
Einstein (1911)	$1+2.5\phi$	$\phi \ll 1;\ \dot{\gamma} \to 0$
Eilers (1941)	$1+\{1.25/[1-(\phi/\phi_m)]\}^2$	
Eilers (1943)	$1+2.5\phi+k_2\phi^2+k_3\phi^3$	$k_1=4.94 \quad k_2=8.78$
Vand (1948)		$k_1=7.39 \quad k_2=16.2$
Habard (1956)		$k_1=6.25 \quad k_2=15.7$
Mooney (1951)	$\exp\{[2.5\phi/[1-(\phi/\phi_m)]\}$	
Krieger and Dougherty (1959)	$\{1-(\phi/\phi_m)\}^{-[\eta]\phi_m}$	$[\eta]$ = intrinsic viscosity
Roscoe (1952)	$(1-\phi)^{-2.5}$	
Ford (1960)	$(1-2.5\phi)^{-1}$	
Ford (1960)	$[1-2.5\phi+11\phi^5-11.5\phi^7]^{-1}$	
Thomas (1965)	$1+2.5\phi+10.05\phi^2+0.00273e^{16.60\phi}$	
Frankel and Acrivos (1976)	$1+(9/8)\{(\phi/\phi_m)^{1/3}/[1-(\phi/\phi_m)^{1/3}]\}$	$\phi \approx \phi_m$
Kitano et al. (1981)	$[1-(\phi/\lambda)]^{-2}$	λ = empirical parameter

because of uncertainties regarding possible viscometer wall and/or end effects, and limited or the absence of any examination of possible shear-dependence effects. The limitations of the functional form in Eq. 27 derive from the fact that volume fraction of solids alone constitutes necessary, but insufficient, information regarding the state of the suspension. Among other important factors are inertia effects, particle size and shape, and size distribution effects, slip and nonbuoyancy effects, and concentration and associated particle-particle interaction effects.

Provided that particle size is within limits imposed by the continuum constraint, absolute particle size is irrelevant within the context of Einstein's treatment and indeed the form in Eq. 27 as well. But we know, for example, that certain particle size mixes are capable of more efficient packing than those consisting of narrow size fractions and further that they can lead to lower effective viscosities for the same overall volume fraction. Furthermore, calculations and experiments suggest that inclusion of even small (that is, linearized) inertia effects (Lin et al., 1970) or anisometric shapes, such as ellipsoids, rods, and disks (Jeffrey, 1922; Pokrovskii, 1967; Clarke, 1967) lead to nonlinear as well as to anisotropic behavior. The theoretical relative viscosity formula:

$$\eta_{r0} = \eta_0/\eta_S = 1 + (9/8)\{(\phi/\phi_m)^{1/3}/[1-(\phi/\phi_m)^{1/3}]\} \quad (28)$$

is important. It gives the zero-shear viscosity η_0 of a suspension of uniform spheres in the concentrated, near-contact limit $\phi \sim \phi_m$ and was derived by Frankel and Acrivos (1967) using the lubrication analogy. An analogous expression for the high-shear-limit viscosity has recently been proposed by Sengun and Probstein (1989).

Empirical non-Newtonian models

A practical scheme for depicting the shear stress (τ) - shear rate ($\dot{\gamma}$) dependence of CWM is through use of empirical rheological models. Plots of τ vs. $\dot{\gamma}$ on logarithmic scales often result in linear regions over limited ranges of shear rate, and these can be described by the two-parameter power-law model given by:

Power-law model:

$$\tau = \tilde{K}\dot{\gamma}^{\tilde{n}} \quad (29)$$

in which $\tilde{K}$ and $\tilde{n}$ are model parameters. Models that incorporate a yield stress value are also useful and include the following:

Bingham plastic:

$$\tau = \tau_b + \eta_p\dot{\gamma} \quad (30)$$

Casson model:

$$\tau^{1/2} = \tau_c^{1/2} + (\eta_c\dot{\gamma})^{1/2} \quad (31)$$

Herschel-Bulkley model:

$$\tau = \tau_h + K_h\dot{\gamma}^n \quad (32)$$

Curve-fitting shear stress-shear rate data to determine τ_b, τ_c, or τ_h will not, and generally does not, insure that a yield stress, as an intrinsic, instrument-geometry indifferent, material property, has been determined or, for that matter, exists. Such curve-fitted values must, unless otherwise confirmed, be viewed as model parameters. The review by Bird et al. (1982) contains compilations of solutions of flows of Bingham plastic and other viscoplastic models. In the present work, we determined yield stresses as model parameters by curve-fitting shear stress-shear rate data to various models, and we also measured the values directly using the vane method.

Shear stress-shear rate dependence and yield stress of CWM

There are many published studies on the viscosity of CWM. By far the vast majority involve reports on single-point, moderate shear rate viscosities using rotational viscometers. The narrow aim of this type of information is essentially limited to screening CWM formulations: its prevalence is a concession to the considerable experimental difficulties associated with obtaining definitive, instrument-geometry indifferent, effective rheological data over broad ranges of shear rates. The shear rate range must be probed because one must, unless otherwise discovered, suppose that such mixtures are rheologically complex. Rotational instruments are generally restricted to modest shear rates. High shear rates are reachable using capillary rheometers; the work is much more tedious.

Alessandrini et al. (1983) used a coaxial cylinder viscometer to measure the flow curves for suspensions of very fine coal with a broad particle size distribution in two organic liquids and in fuel oil, covering a range of shear rates from about 50 to 10^3 s^{-1}. They found the dependence to be related to the nature of the suspending liquid, and to involve an apparent yield stress and to be describable by the Herschel-Bulkley model, Eq. 32, for trimethylphosphate and by the power-law model for dibutylphosphate and fuel oil. Woskoboenko et al. (1987) measured the flow curves for aqueous slurries of fine, broad-particle size Victorian brown coal (very high moisture and abundant in Australia) in a Couette viscometer over the range from about 1 to 800 s^{-1}. They correlated the data using the Bingham plastic model, Eq. 30. The Bingham yield stress parameter τ_b was correlated with solids volume fraction through a power function of the mean interparticle separation, approximated using the capillaric model of the slurry, which additionally involves the specific external surface area of the particles. Inasmuch as interparticle separation does not vanish at maximum packing when the capillaric model is used, though it attains a minimum value, the correlation does not give the expected limiting value $\tau_b \to \infty$ as $\phi \to \phi_m$.

Tsai and Knell (1986) measured the flow curves for polymer-stabilized aqueous slurries of two monomodal fine coals of broad particle size distributions, using both rotational and capillary rheometers, which permitted a combined shear rate range of about 1 to 10^4 s^{-1}. They found the behavior to be power-law shear-thinning and possessing a yield value. Some of their apparent viscosity-shear rate data points for different capillary-tube diameters had a lot of separation, raising suspicion of the possible presence of wall-slip effects. This work is distinguished by its attempt to cover a large range of shear rates, though the lower limit of the measured range could not

Table 3. Properties of Pittsburgh Seam No. 8 Coal

Coal Analysis	As Received	Moisture Free	Dry and Ash Free	Min. Mat Free Dry	Min. Mat Free Moist
Moisture	1.5				1.7
Volatile Matter	36.2	36.7	39.7	39.0	38.3
Fixed Carbon	54.9	55.8	60.3	61.0	60.0
H-T Ash	7.3	7.4			
Hydrogen	5.6	4.97	5.37		
Carbon	74.79	75.94	82.05		
Nitrogen	1.53	1.55	1.68		
Oxygen	9.63	8.41	9.08		
Sulfur	1.66	1.69	1.82		
H-T Ash	7.33	7.44			
Sulfate Sulfur	0.05	0.05	0.55		
Pyrite Sulfur	1.00	1.02	1.10		
Organic Sulfur	0.61	0.62	0.67		
Total Sulfur	1.66	1.69	1.82		
Total Chlorine	0.130	0.132	0.143		
Btu/lb	13,540.0	13,749.0	14,855.0	15,010.0	14,760.0
$J/kg \times 10^{-7}$	3.149	3.198	3.455	3.491	3.433
Gieseler Plasticity		(0.5 Div./min) Softening Temp.		393.0	
		Max. Fluidity Temp.		420.0	
		Solid Temp.		441.0	
		(Div./min) Max Fluidity		6.0	
Free Swelling Index		7.5			
Thermal Conductivity		0.260 W/m·K			
Heat Capacity		0.33 cal/g·K			

conceivably be anywhere near 0 s^{-1} as claimed. Leong et al. (1987) measured the flow curves for Australian brown coal slurries of broad particle size distributions, using a capillary rheometer and presheared mixtures as the slurries had time-dependent behavior. They also measured the yield stresses using the vane method as a function of suspension mixing/resting cycles. They found the behavior to be Newtonian for low solids loadings, shear-thinning non-Newtonian for intermediate concentrations, and non-Newtonian with a yield stress for high solids loadings.

Description of New Work

Test materials and particle characterization

The coal used in our studies was a Pittsburgh Seam no. 8 bituminous coal obtained in dry granular form from Consolidation Coal Company. It was separated into four size ranges using sieves and a sieve shaker; the different fractions were stored in sealed plastic bags until sufficient test samples had been collected. Coal slurries were made up using distilled water, and concentration was varied by adding or removing supernatant liquid. Detailed characterization of the coal included proximate and elemental analyses, determination of heating value, measurement of heat capacity, and determination of effective solid thermal conductivity. These properties are listed in Table 3. The solid densities for each particle size fraction were determined using calibrated pycnometers with a temperature bath at 25°C. A 0.01% solution of Triton X-100 was used as a wetting agent in these density measurements, but no additives were used in making up any of the test slurries. The particle size distribution of the four test size fractions were determined using our Particle Data Labs. Computerized Elzone Counter.

The principle and the operation of this instrument, which is based on the electrical sensing zone method, are described by Allen (1975). There are two important attributes: one regarding the method and the other regarding the special capability of our instrument. The electrical sensing zone method determines the volume-equivalent particle diameter, and our instrument typically samples a very large population of particles, from about 19,500 to over 191,000 for the data reported here. The measured particle sizes are given in the form of frequency and of cumulative distributions in Figures 1 and 2, respectively. Calculated mean particle sizes and other statistical attributes of the size distributions are listed in Table 4. It is evident from the closeness in values of the various means and the fairly small values of the standard deviations relative to the associated means (the coefficients of variation, C.V.) that the distributions for the three larger size fraction coal samples are fairly narrow. The distribution for the -325 mesh particle size fraction is broad.

In addition to these measurements, we determined the maximum packing volume fractions, ϕ_m, for all four size fractions of our coals by centrifugation. Our procedure involved centrifuging small, concentrated slurry samples at 8,000 rpm (corresponding to a relative centrifugal force, RCF, of 6,550 G for our rotor) for one hour, removing the excess supernatant and then centrifuging the sediment again for an additional hour. After this, the remaining excess supernatant, which was quite small, was removed and the sediment was weighed wet and after drying for 24 hours at 80°C. The maximum packing volume fractions, ϕ_m, and weight fractions, ω_m, of solids determined in this way are listed in Table 4.

Settling rates of CWM

Sedimentation experiments were performed in 500-mL graduated cylinders, having diameters of 4.66 cm at 25°C in a

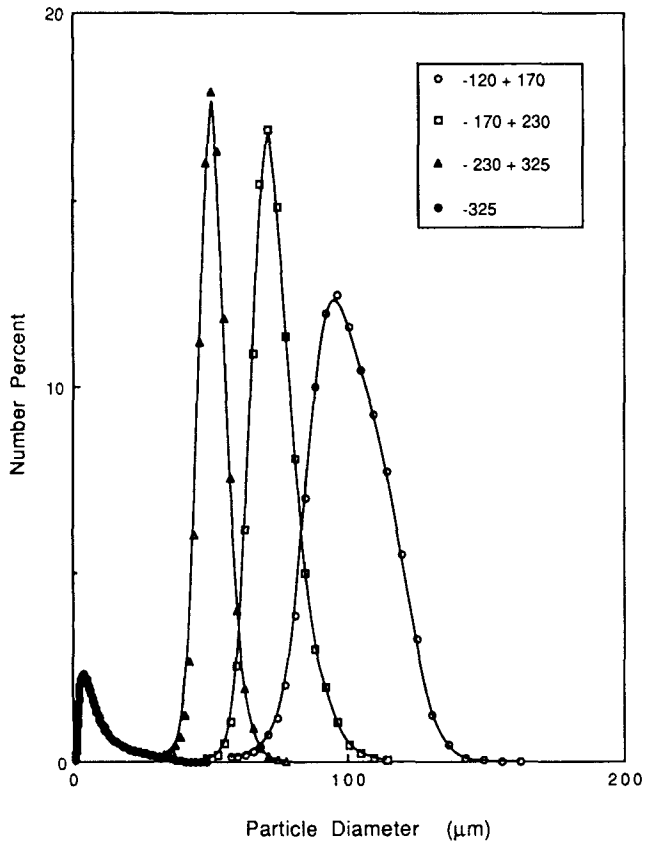

Figure 1. Particle size distributions for coal particles: frequency plots.

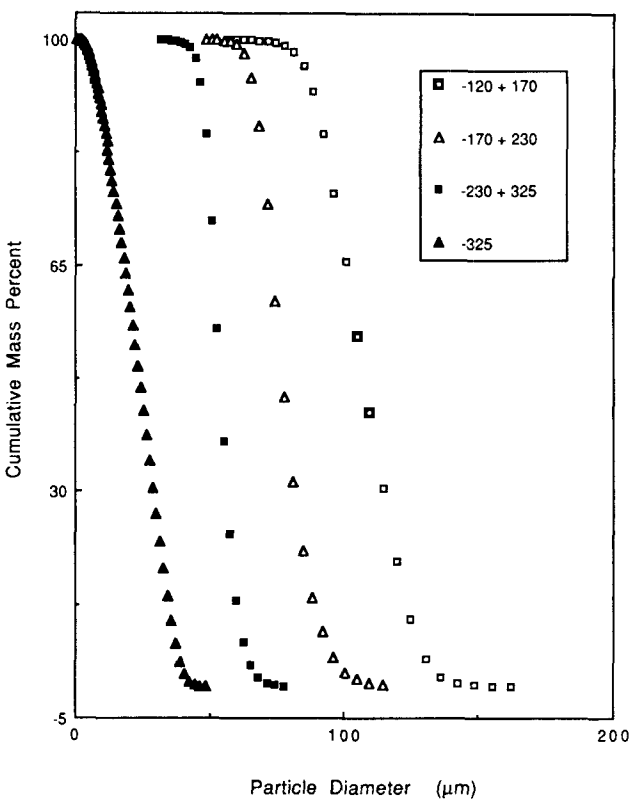

Figure 2. Particle size distributions for coal particles: cumulative plots.

constant temperature bath using different initial concentrations of the suspensions. The procedure involved bringing the test slurries to experimental temperature, filling the cylinders, covering them, redispersing the solids by inverting the cylinders at least 20 times, and replacing them into the constant temperature bath. The settling rates were then determined by recording the height of the descending interface as a function of time. The settling-rate curves for the 120/170 mesh coal slurries are given in Figure 3, which indicate that constant-rate sedimentation is rapidly and unambiguously established for suspensions with this particle size coal and that it persists until

Table 4. Properties and Size Analysis of Coal Particles

Coal sample	120/170	170/230	230/325	−325
ρ_s(g·cm^{-1})	1.3387	1.3401	1.3408	1.3454
ϕ_m(v/v)	0.538	0.531	0.516	0.628
ω_m(w/w)	0.610	0.598	0.589	0.694
	Mean Particle Diameters (μm)			
$\bar{d}$	99.6	73.2	50.9	5.7
$(\bar{d^2})^{1/2}$	100.6	73.7	51.2	7.6
$(\bar{d^3})^{1/3}$	101.5	74.2	51.5	9.9
$(\bar{d^2}/\bar{d})$	101.5	74.2	51.5	10.2
$(\bar{d^3}/\bar{d})^{1/2}$	102.4	74.7	51.8	13.0
$(\bar{d^3}/\bar{d^2})$	103.3	75.2	52.1	16.5
$(\bar{d^4}/\bar{d^3})$	105.0	76.3	52.7	22.2
d_{N50} (number-median)	101.6	73.4	51.8	4.1
d_{M50} (mass-median)	107.0	76.7	53.2	23.1
	Standard Deviations (μm)			
σ_N	14.1	8.6	5.5	5.0
C.V.%*	14.1	11.7	10.8	87.7
σ_M	13.7	9.6	5.1	9.5
C.V.%**	13.0	12.6	9.7	42.8

*C.V.% = $[\sigma_N/\bar{d}] \times 100$

**C.V.% = $[\sigma_M/(\bar{d^4}/\bar{d^3})] \times 100$

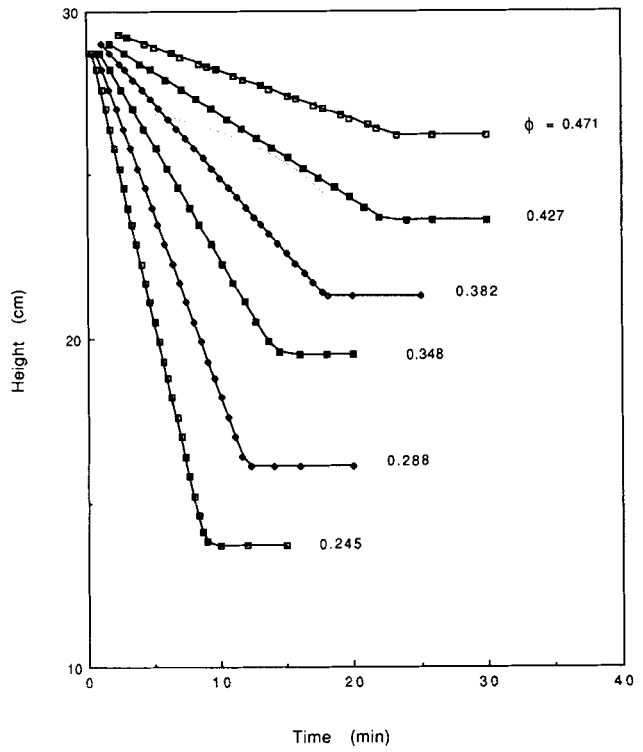

Figure 3. Settling rate curves for 120/170 mesh coal slurries at 25°C.

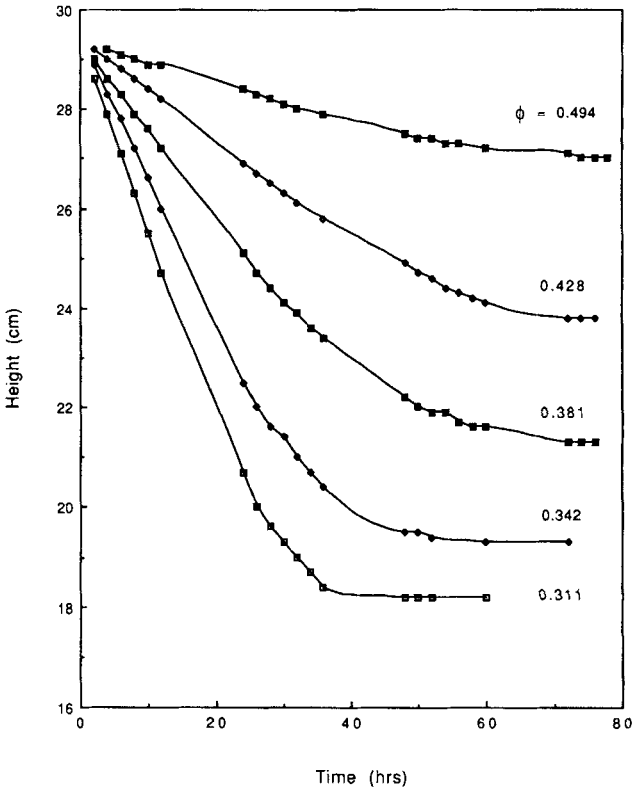

Figure 4. Settling rate curves for −325 mesh coal slurries at 25°C.

all particles have settled. The settling-rate curves for the slurries made up of the next two smaller test particle size fractions, the 170/230 mesh and the 230/325 mesh coals, were found to be qualitatively identical to those in Figure 3 with regard to the rapidity and certainty of the establishment of constant-rate sedimentation, as well as its persistence to the end of the settling, except, of course, that the rates of descent of these smaller particles were slower. Furthermore, the final sediments for all these slurries were found to be relatively incompressible, being essentially unaffected by the extent of buoyed weight of solids and embodying solid volume fractions within 2% of the values corresponding to maximum packing.

By contrast, the curves for the slurries made up of the smallest particle size fraction, the −325 mesh coal, given in Figure 4, suggest that the settling rate decreases as sedimentation progresses and that the final sediments are relatively compressible. The latter observation is re-affirmed by the finding that the final sediments from gravity settling for this particle size were affected more strongly by the buoyed weight of solids and that the volume of solids they contain are lower by from about 12 to 33% than the value corresponding to maximum packing.

Table 5 lists the results of fitting the settling rate data for all of our coal-water mixtures to Eqs. 17 and 33. The values of n in Richardson and Zaki's equation, Eq. 17, range from about 5.74 to about 6.55 (for the −325 mesh slurry), which are significantly larger than the accepted value of about 4.68 for hindered settling of spherical particles and indeed larger than the values obtained by Chong et al. (1979) for cubic and angular particles. These results demonstrate that the nonspherical shapes of the coal particles and, in the case of the smallest particle size test coal, especially, the relatively broader size distribution of particles, lead to significant further retardation of the settling. The values of κ in Table 5 are calculated from the settling-rate data using a variant of Eq. 17 that incorporates an "effective volume fraction" $\kappa\phi$ of particles as:

$$U = v_t(1 - \kappa\phi)^{4.68} \tag{33}$$

Table 5. Hindered Settling Parameters for CWM

Test Coal Mesh Size	n	$v_\infty \times 10^3$ (cm·s^{-1})	d_{St} (μm)	κ	$v_\infty \times 10^3$ (cm·s^{-1})	d_{St} (μm)
	Equation 17			Equation 33		
120/170	5.92	208.0	99.8	1.15	182.0	93.5
170/230	5.95	113.0	73.2	1.15	99.0	68.7
230/325	5.74	53.0	50.2	1.13	48.0	47.5
−325	6.55	1.9	9.5	1.20	1.5	8.3

Table 6. Calculated Particle Shape Factors from Sedimentation Data

Coal Sample		120/170	170/230	230/325	−325
d_{St} (μm)	Eq. 17	99.8	73.2	50.2	9.5
$d_D \approx \bar{d}^3/d_{St}^2$ (μm)	Eq. 4	99.2	73.2	52.3	2.05
$\psi \approx (d_{St}/\bar{d})^4$	Eq. 5	1.008	1.000	0.946	7.72
$K = (d_D/d)$	Eq. 12	0.996	1.000	1.028	0.360
$1/k$	Eq. 13	0.996	0.999	1.020	0.571
d_{St} (μm)	Eq. 33	93.5	68.7	47.5	8.3
$d_D \approx \bar{d}^3/d_{St}^2$ (μm)	Eq. 4	113.0	83.1	58.4	2.69
$\psi \approx (d_{St}/\bar{d})^4$	Eq. 5	0.777	0.776	0.758	4.50
$K = (d_D/d)$	Eq. 12	1.135	1.135	1.147	0.472
$1/k$	Eq. 13	1.101	1.101	1.112	0.644

These values of κ provide measures of the degree of augmentation of the volume fraction associated with the amount of fluid entrained by the nonspherical, settling coal particle. It is found again that for the three larger (and relatively narrower) particle size fractions, this value amounts to approximately 15%, but it is measurably larger for the smallest (and relatively broadest) particle size fraction for which it is 20%. This is perhaps due to the additional entrapment of fluid within particle aggregates that are more likely to form with the smaller particles.

Both Eqs. 17 and 33 seem to result in equally satisfactory fits of the experimental settling rate data for our coal slurries, predicting settling rates with average absolute deviations of less than 4%. The calculated single-particle settling velocities v_t from Eq. 17 are somewhat larger than those from Eq. 33, but in either case they do not differ, well within experimental error, from the corresponding free-settling velocities, v_∞, because the calculated wall correction from Eqs. 23-25 in the worst case (for the 120/170 mesh particles) is less than 0.5%. These free-settling velocities were used to calculate the effective Stokes diameters d_{St} using Eq. 2. These are also listed in Table 5 and will be examined further. We also used the free-settling velocities from Table 5 to calculate the corresponding single-particle Reynolds numbers, and in turn they were used to calculate the hindered-settling indices n using the applicable relation from Eqs. 18-21 of Richardson and Zaki, as well as Eq. 22 recommended by Garside and Al-Dibouni. These calculated values of n were found to range from 4.65 to 4.69 for the former set of equations and from 5.04 to 5.10 for Eq. 22. Accordingly, both relations underestimate the real hindered settling indices for our test slurries, which may suggest that our slurries fall outside the range of Richardson and Zaki's relation.

Aside from the foregoing, we used the single-particle Stokes diameters from Table 5, which are based on sedimentation data to deduce shape parameters for our particles using relationships quoted before. It was noted that the particle diameter measured using the electric sensing zone principle is the equivalent spherical volume diameter, d_V, and inasmuch as the distributions for our three larger particle size fractions were fairly narrow we take $d_V = \bar{d}$. This permits us to estimate the drag diameters and the sphericities for our particles using the approximations in Eqs. 4 and 5, respectively, the McNown and Malaika (1950) shape factor K from Eq. 12, and the shape factor $k(=1/K)$ using the empirical correlation of Pettyjohn and Christiansen in Eq. 13. Several inferences can be made from an examination of these results, see Table 6. First, it appears that the dispersion of sizes for our smallest particle size fraction coal (−325 mesh) is too broad for the mean particle diameter $\bar{d}$ to provide a meaningful representation for the equivalent volume diameter d_V for use in relationships applicable strictly to monodispersed particle sizes, such as Eqs. 4, 5, 12 and 13. Therefore, the results in Table 6 pertaining to this coal size fraction do not have any significance.

For the three larger coal particle size fractions, however, the estimated drag diameters and shape factors, calculated on the basis of the Stokes diameter derived from analyzing the concentrated settling-rate data according to Richardson and Zaki's correlation turn out to be essentially those of a sphere having the mean particle diameter $\bar{d}$. That is, all different equivalent spherical diameters, d_{St}, d_D, and $\bar{d}$, are essentially the same, and all shape factors are approximately unity. Therefore, except for a marked increase in the value of the hindered settling index n over that pertaining to spheres, derived results using this correlation are evidently indifferent to nonsphericity of particle shape. In contrast, the results based on Stokes diameters derived from analyzing the concentrated settling-rate data using the correlation involving the effective volume concept, Eq. 33, lead to different conclusions. In this case, the particle sphericities for the three larger size fraction coals are found to be about 0.77, while the shape factors K from Eq. 12 are found to be about 1.14. The reciprocal values k calculated from the approximation given by Eq. 13, using these calculated sphericities, are found to have the slightly smaller value $1/k(=K) \approx 1.1$. Reference to McNown and Malaika's article will indicate that values of K in the range of $1.10 \le K \le 1.15$ define a narrow geometric region bracketed by roughly the following ranges of values among the three ellipsoidal semi-axes a, b, c: $1 \le (b/c) \le 5$ and $1/2 \le a/\sqrt{bc} \le 8$. A variety of particle shapes are subsumed within this region, from oblate spheroids through ellipsoids to prolate spheroids. The value of the sphericity constitutes a constraint that is invoked to establish a relationship among the three size parameters, a, b, and c. For oblate ($a < b = c$) or prolate ($a > b = c$) spheroids, the sphericity is sufficient to provide all ratios among these parameters; the particle volume diameter is then used to establish their absolute numerical values. Our interpretation of these shape data is given next.

Rotation-free terminal velocities are attainable for ellipsoids and for bodies of revolution with sufficient symmetry, but the

velocities will depend on the orientation. Asymmetric particles will not fall vertically in all orientations, but will tend to drift sideways, unless the motion starts with a principal axis aligned with the direction of gravity. Accordingly, a given particle can have a range of settling velocities, particularly if it is highly nonisometric, but the range is usually rather limited. Of special interest here is the finding by Heiss and Coul (1952) that the ratio of extremes of fall velocities were limited to within 2 for discs and cylinders with diameter-to-length ratios varying from 1 to as high as 10. Photomicrographs of our pulverized coals, which provide the projected particle profiles, indicate that they have roughly equidimensional, albeit irregular, shapes not incompatible with the shape factors obtained here.

If we assume that the particles are disc-shaped, we find that a sphericity of 0.77 corresponds to discs of thickness-to-diameter ratios of about 0.357. Alternatively, if the particles are assumed to be oblate spheroidal with $b(=c)$ taken as the major semi-axis of the projected ellipse, the minor semi-axis value corresponding to a particle sphericity of 0.77 is given by $a=0.585\,b$. These give $(b/c)=1$ and $(a/\sqrt{bc}\,)=0.585$ which correspond to $K=1.1003$, as calculated using analytical expressions given by McNown and Malaika (1950, Eq. 5 in Table 1). Therefore, not only do the calculated shape factors ψ and K, as interpreted here, provide the relevant particle shape effect, but they also do so in a consistent way. Some of the coal particles are very slightly elongated; these can be described by taking the shape to be ellipsoidal (with all semi-axes assumed to differ) and relationships among them established by enforcing the sphericity value as well as constraints on the permitted range of their ratios.

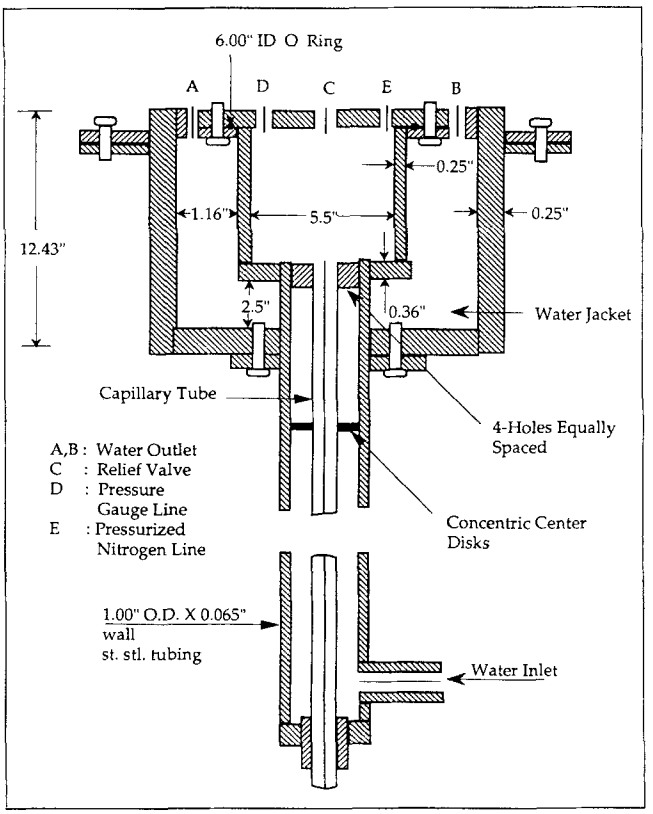

Figure 5. Capillary viscometer reservoir.

Shear stress-shear rate and yield stress data for CWM

The shear stress-shear rate dependences of the test suspensions were measured using a capillary rheometer designed and constructed in our laboratory. The main body of the instrument in Figure 5 consists of a cylindrical stainless steel reservoir of 5.5-in. (140-mm)-ID 9.6-in. (244-mm)-high and 0.25-in. (6.4-mm) wall thickness. The reservoir is mounted inside a cylindrical jacket providing a 1.16-in. (29.5-mm)-wide annular clearance for circulation of water from a constant temperature bath. A large set of capillary tubes, made from precision-bore stainless-steel tubing in at least two lengths for each diameter and covering the range of nominal diameters from 3/32 to 11/32 (2.4 to 8.8 mm) were machined for use with the instrument. Each tube is fabricated with appropriate external spacers to fit centered inside a jacket, which slips through the bottom of the reservoir jacket to form an integral path for circulation of constant temperature water around the capillary tube and then around the slurry reservoir. All tube diameters were calibrated by direct measurement using mercury filling and checked indirectly by viscosity measurement using Newtonian viscosity calibration fluids. The reservoir cover consists of a 0.25-in. (6.4-mm)-thick stainless-steel flange with ports for connection to a gas cylinder, a vacuum pump and a series of pressure transducers, and for insertion of a thermocouple, a siphon tube, and a stirrer shaft.

The pressure transducers are connected to a Validyne demodulator for conversion of the signal into digital form. Stirring is done using two impellers on the stirrer shaft, a turbine impeller at the bottom, and a marine-type impeller at the top, and the stirring speed is varied by a speed controller. Slurry flow rate is determined automatically by collecting the effluent from the capillary tube in a container that rests on a Setra 5,000 electronic balance equipped with an RS 232 port connected serially to an IBM XT PC whose internal clock is used as a timer. For any given run, suspension temperature and density and tube dimensions are entered into the PC, and the pressure and flow rate are directly recorded and stored in a computer database for later retrieval and analysis. In addition, the PC is linked to the University's mainframe. The entire capillary rheometer assembly including all ancillary devices are shown in Figure 6.

For a given slurry the shear stress-shear rate dependence, τ vs. $\dot{\gamma}$, is calculated from the experimentally measured pressure drop-volumetric flow rate data, ΔP vs. Q, corrected for possible end and/or wall-slip effects, using the Rabinowitsch-Mooney relations which gives the shear rate value at the tube wall:

$$\dot{\gamma}=\left(-\frac{du}{dr}\right)_w=\frac{3n'+1}{4n'}\,(8V/D) \tag{34}$$

in which

$$n'=d\log(D\Delta P/4L)/d\log(8V/D) \tag{35}$$

where $V=(4Q/\pi D^2)$ is the average velocity, and D is the tube diameter. The shear stress value at the wall corresponding to $\dot{\gamma}$ is given by:

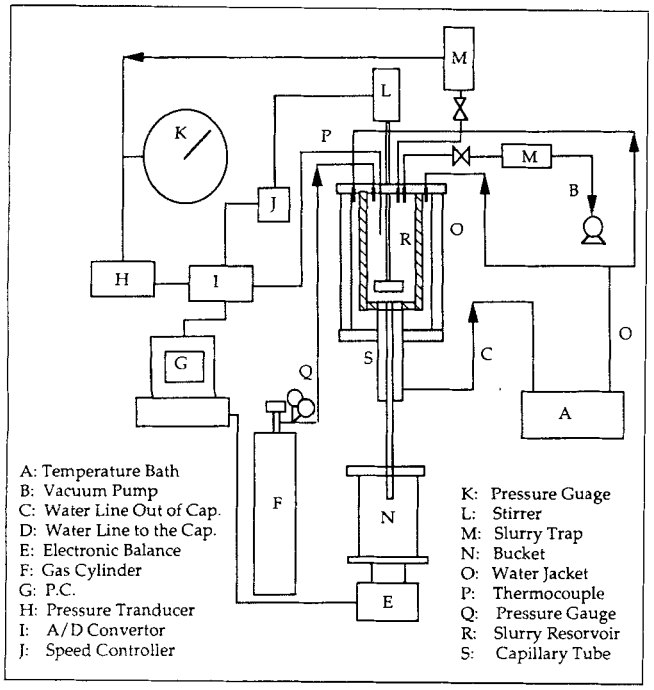

Figure 6. Capillary viscometer system.

$$\tau = (D\Delta P/4L) \tag{36}$$

Equations 34-36 form the basis for the calculation of the shear-stress/shear-rate curves for our coal slurries from the corrected pressure-gradient/flow-rate data. Details of the correction procedures and the calculation program are given by Attal (1989). We note that $(8V/D)$ is called the apparent shear rate, since it only strictly gives the value of the wall shear rate for a Newtonian fluid, for which $n' = 1$.

We also determined the yield stresses of our CWM by direct measurement. The direct method used in our work for measurement of the yield stress was the vane method (Nguyen and Boger, 1983). The vane element consists of four thin rectangular blades attached, at right angles to each other, to a thin, rigid, central, cylindrical shaft. The element is driven by our Brookfield viscometer motor. The experiment entails recording the torque history, as the immersed element is rotated at a very low speed. The yield stress is determined from the maximum in the torque-time curve that corresponds to the point of yielding. Description and verification of the method, its origin in the traditions of soil testing, and the basic equations for calculating the yield stress are presented by Nguyen and Boger (1983) and Dzuy and Boger (1985). Additional details on our apparatus and further testing and validation of the method are given by Avramidis and Turian (1991).

The shear stress vs. shear rate results for different concentrations of the CWM made up of the four sizes of coal particles are given in Figures 7-10. It is clear that for slurries made from the three larger particle sizes, Figures 7-9, the plots are straight lines over the measured range of $\dot{\gamma}$ of approximately between 1 and $10^4\,s^{-1}$, suggesting power-law behavior described by Eq. 29. The calculated power-law parameters, the consistency index $\tilde{K}$ and the flow behavior index $\tilde{n}$, for these slurries are given in Table 7. The flow behavior index values, $\tilde{n}$, for

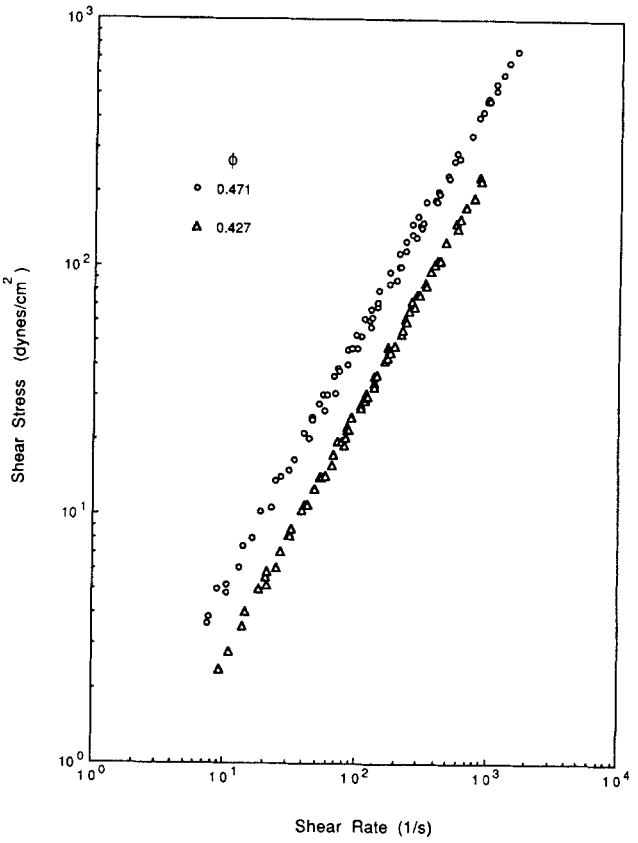

Figure 7. Shear stress-shear rate curves for 120/170 mesh CWM at 25°C.

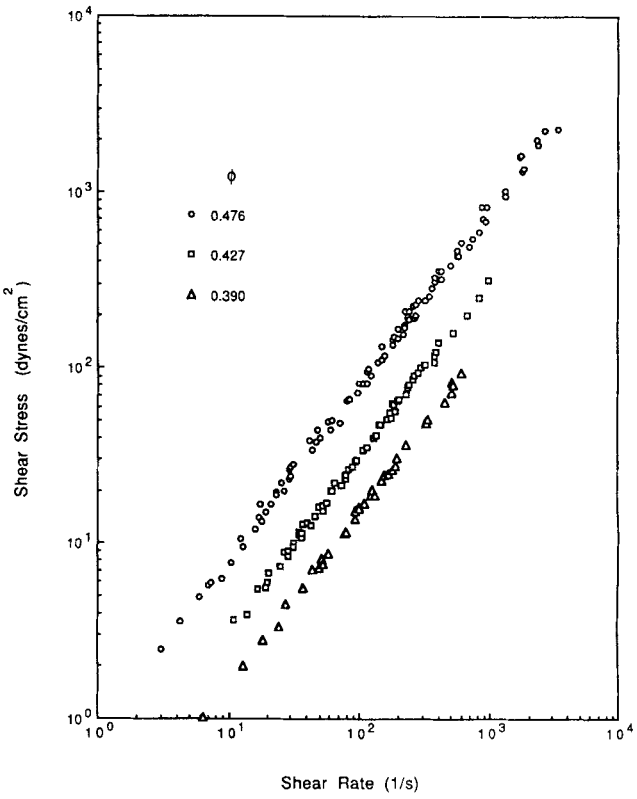

Figure 8. Shear stress-shear rate curves for 170/230 mesh CWM at 25°C.

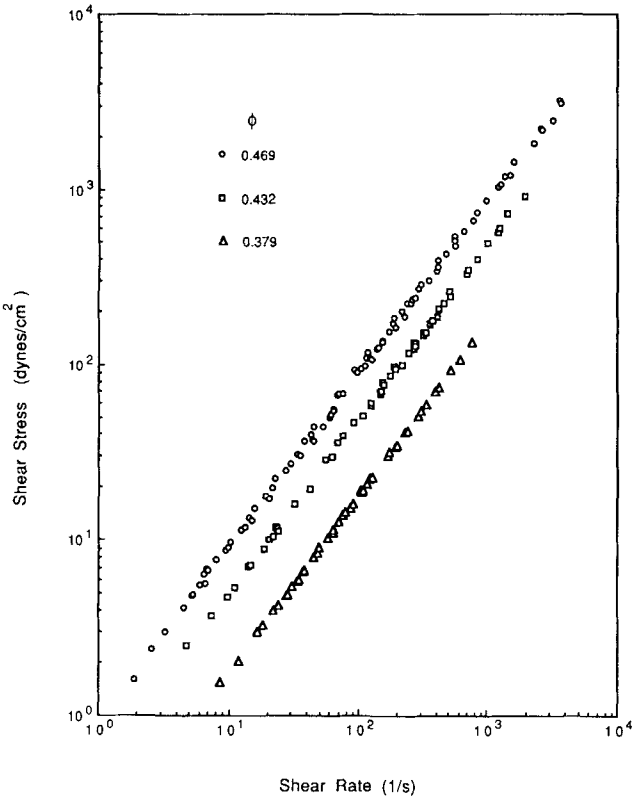

Figure 9. Shear stress-shear rate curves for 230/325 mesh CWM at 25°C.

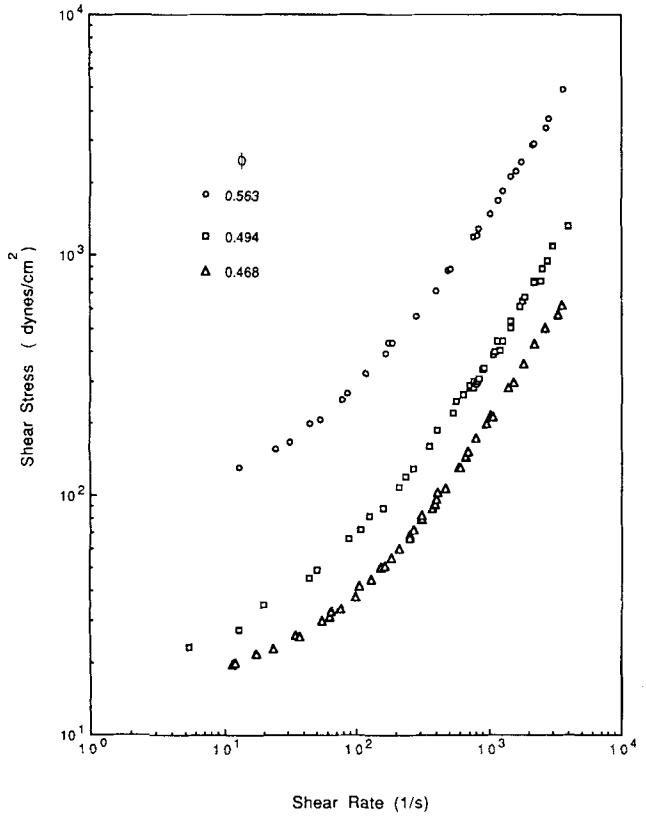

Figure 10. Shear stress-shear rate curves for − 325 mesh CWM at 25°C.

Table 7. Power-Law Parameters and Newtonian Viscosities of CWM

			Equation 29		
Coal Sample	ω (w/w)	ϕ (v/v)	$\tilde{K}^*$	$\tilde{n}$	μ (poise)
120/170	0.500	0.427	0.301	0.96	0.264
	0.545	0.471	0.697	0.98	0.631
170/230	0.462	0.390	0.149	1.01	0.152
	0.500	0.427	0.298	1.02	0.319
	0.550	0.476	0.835	0.98	0.837
230/325	0.451	0.379	0.182	0.99	0.178
	0.506	0.432	0.505	0.99	0.512
	0.543	0.469	1.08	1.01	0.982

*$\tilde{K}$ has units of $g \cdot cm^{-1} \cdot s^{\tilde{n}-2}$.

these suspensions are all very near unity, well within the slight scatter of the data. We tried, in vain, to extend measurement of the flow behavior for these three sizes of coal to lower shear rates than those depicted in Figures 7-9, but it was impossible to maintain a uniform concentration of solids in the effluent slurry stream, that is, one equal to that charged to the reservoir. We also determined the Newtonian viscosities, μ, pertaining to the entire measured range using least squares fits to these data, as shown in Table 7. Furthermore, for these slurries, made with the three larger size fraction coals, yield stresses using our vane apparatus were not measurable; while the corresponding flow curves obtained using the capillary rheometer provide no clue that they exist, it is possible that their magnitudes are below detection limits of our instrument.

The flow curves for the slurries made using the − 325 mesh coal particles are strongly non-Newtonian. Figure 11 presents the viscosity vs. shear rate plots for these slurries. It is evident that the behavior is shear-thinning with a steep slope at the low end, suggesting the existence of a yield stress and tending toward a high-shear Newtonian limit at the high end. We also measured the yield stress-concentration dependence for the slurries made from the − 325 mesh coal particles using the vane method. These yield stress data are listed in Table 8.

Yield stress concentration dependence of CWM

The yield stress-concentration dependences for the CWM made of the − 325 mesh particle coal were correlated using the following two τ_0-ϕ correlation forms:

$$\tau_0 = \frac{\tau^*(\phi/\phi_m)^2}{[1-(\phi/\phi_m)^{1/3}]^\beta} \tag{37}$$

and

$$\tau_0 = \tau_* \left[\frac{(1-\phi_m)(\phi/\phi_m)}{1-(\phi/\phi_m)}\right]^\zeta \tag{38}$$

in which τ^*, β, τ_*, and ζ are positive parameters. In each of these correlations, the maximum packing solids volume fraction, ϕ_m, is the value estimated independently by centrifugation. The common idea behind these two equations is that the yield stress depends on some function of the mean interparticle spacing as one of the primary variables. Equation 37 incor-

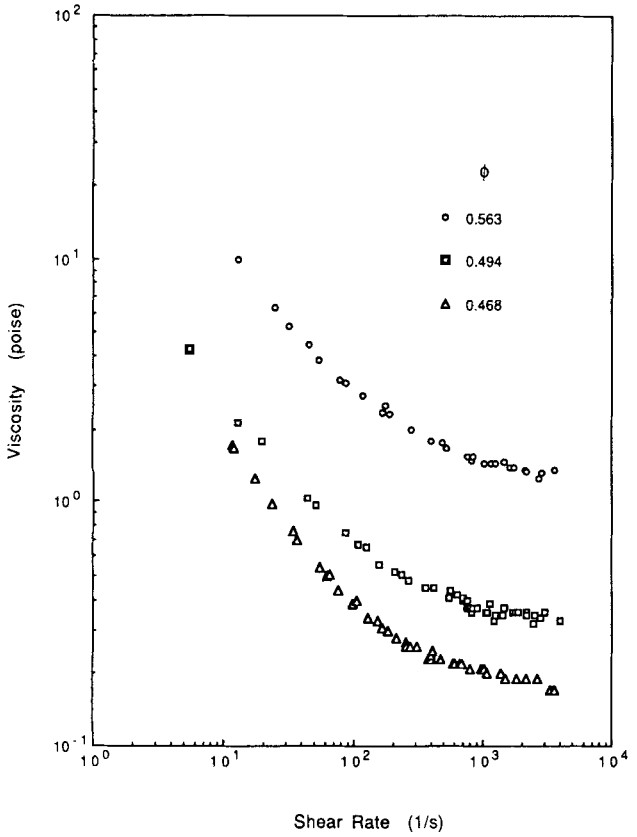

Figure 11. Viscosity-shear rate curves for −325 mesh CWM at 25°C.

porates a dimensionless mean particle spacing based on a simple cubic lattice particle arrangement, in which the particles, assumed to be uniform spheres, occupy the centers of cubic cells of fluid. For such an assumed particle packing, $[1-(\phi/\phi_m)^{1/3}]$ is the dimensionless ratio of particle spacing to that of the side of the cell. In this case, particle spacing vanishes at maximum packing.

Alternatively, Eq. 38 embodies the mean particle spacing derived on the basis of the capillaric model of the slurry. Here, the equivalent capillaric diameter gives the distance between solid surfaces, but it does not vanish at maximum packing; it attains a minimum. Accordingly, the reciprocal of the quantity in square brackets in Eq. 38 is the excess over that at maximum packing of the ratio of the capillaric diameter at the prevailing solid concentration to that at maximum packing. Of course, this vanishes at maximum packing. We have used Eq. 37 previously to describe the yield stress-concentration dependences of laterite slurries (Avramidis and Turian, 1991). It was indicated there that the term $(\phi/\phi_m)^2$ in the numerator in Eq. 37, being dominant in the dilute limit, is suggested by dilute limit theory, while the term involving the parameter β in the denominator is dominant in the concentrated limit $(\phi/\phi_m)\approx 1$. The limiting forms of Eqs. 37 and 38 in the dilute and concentrated limits are useful in revealing the roles played by the various coefficients in these relationships. For $(\phi/\phi_m)\ll 1$, the limiting form of Eq. 37 is given by the expansion:

$$(\tau_0/\tau^*)\approx\chi^2\left[1+\beta\chi^{1/3}+\frac{\beta(\beta+1)}{2}\chi^{2/3}+O(\chi)\right] \quad \text{for } \chi=(\phi/\phi_m)\ll 1 \qquad (39)$$

and that of Eq. 38 is given by the expansion:

$$(\tau_0/\tau_*)\approx[(1-\phi_m)\chi]^{\zeta}\left[1+\zeta\chi+\frac{\zeta(\zeta+1)}{2}\chi^2+O(\chi^3)\right] \quad \text{for } \chi=(\phi/\phi_m)\ll 1 \qquad (40)$$

The asymptotic form in the limit $(\phi/\phi_m)\approx 1$ for Eq. 37 is given by:

$$(\tau_0/\tau^*)\approx\left(\frac{1-\chi}{3}\right)^{-\beta}\left[1-\left(2+\frac{\beta}{3}\right)(1-\chi)+O(\{1-\chi\}^2)\right] \quad \text{for } \chi=(\phi/\phi_m)\approx 1 \qquad (41)$$

Table 8. Yield Stress-Concentration Dependence for −325 Mesh CWM

ω w/w	ϕ v/v	Yield Stress, dyne·cm^{-2}		
		Expt.	Eq. 37*	Eq. 38**
0.509	0.436	9.0	13.0	12.8
0.546	0.473	21.3	25.1	24.5
0.558	0.485	37.1	31.5	30.9
0.574	0.501	47.6	43.5	43.0
0.585	0.513	60.1	56.7	56.2
0.591	0.519	69.5	65.6	64.9
0.598	0.526	80.7	77.7	77.3
0.605	0.533	99.7	92.9	92.9
0.610	0.539	122.1	110.1	109.8
0.618	0.547	154.9	139.6	139.4
0.627	0.556	191.4	184.3	186.9
0.633	0.563	256.7	234.1	240.2
0.646	0.577	376.4	406.5	431.0
0.662	0.594	796.8	996.2	976.7

* With $\tau^* = 0.319$ and $\beta = 2.05$.
** With $\tau_* = 18.58$ and $\zeta = 2.188$.

and that for Eq. 38 by:

$$(\tau_0/\tau_*)=\left(\frac{1-\chi}{1-\phi_m}\right)^{-\zeta}[1-\zeta(1-\chi)+O(\{1-\chi\}^2)]$$

$$\text{for } \chi=(\phi/\phi_m)\approx 1 \quad (42)$$

Equations 39 and 40 demonstrate that the factors in the numerators of our yield stress correlations are dominant in the dilute limit; Eqs. 41 and 42 indicate that the denominator terms are important in the concentrated limit. The parameter τ^* or τ_* provides the value of the yield stress corresponding to the circumstance when numerator and denominator concentration-dependent factors in Eq. 37 or 38 are equal: it corresponds to the yield stress demarcating dilute from concentrated behavior. If it were assumed to occur for a solids concentration ϕ^* for Eq. 37 and ϕ_* for Eq. 38, then these are given by:

$$\phi^*/\phi_m=[1-(\phi^*/\phi_m)^{1/3}]^{\beta/2} \quad (43)$$

and

$$\phi_*/\phi_m=1/(2-\phi_m) \quad (44)$$

The comparisons between experiment and Eqs. 37 and 38 are given in Table 8. For Eq. 37 the model parameters obtained by least squares fit of the data are $\tau^*=0.319$ dyne·cm^{-2}, $\beta=2.05$, and $\phi^*=0.196$. The least-squares-fitted parameter values for Eq. 38 are: $\tau_*=18.58$ dyne·cm^{-2}, $\zeta=2.188$, and $\phi_*=0.457$. Equations 37 and 38 appear to do essentially an equally good job of describing the yield stress-concentration dependence; in the present case, both equations predict the data with an absolute average deviation of 12.4%. Furthermore, comparison of the limiting forms of these equations, Eqs. 39-42, suggests that they both lead to effectively similar asymptotic forms in corresponding limits, since the exponents β and ζ turn out to be approximately the same, and both are nearly equal to 2. The values of the transition concentrations, calculated from Eqs. 43 and 44, however, are quite different.

The significance of such yield stress correlations resides in the fact that they provide one quantitative procedure for classifying CWM. Since ϕ_m is determined from the irreducible sediment volume, presumed to correspond to most efficient packing, it is a geometric property of the particle mix and not of chemistry in our scheme. For any particle mix, ϕ_m constitutes the intrinsic limit to solids loading, near which the yield stress becomes impractically large. However, the rate of approach to such large values, given by the slope of the yield stress-concentration curve, depends on the chemistry of the suspension as well, which affects the values of the model parameters in Eqs. 37 and 38. Indeed, the larger the values of the model parameters τ^*, β, τ_*, and ζ, the steeper the approach to infinite yield stress as ϕ approaches ϕ_m. Accordingly, using the yield stress as a guideline in preparing a coal-water fuel (CWF), for example, one would formulate a particle size mix maximizing ϕ_m, a solids concentration near ϕ_m, and a suspension chemistry giving the least steep slope for ϕ near ϕ_m. The effect of suspension chemistry on the model parameters τ^* and β has been studied by Avramidis and Turian (1991).

Viscosity-concentration dependence of CWM

It was indicated that the shear-stress/shear-rate behavior of the CWM made from the three larger particle size coals was found to be essentially Newtonian over the entire measured range of shear rates. Least-squares curve fits of the shear-stress/shear-rate data over the entire measured range of shear for all these suspensions suggest that a Newtonian fluid describes them somewhat better than the (slightly) power-law model, with approximately the same absolute average deviations; they ranged from 1.6 to in only one case about 25% depending on the suspension. The relevant Newtonian viscosities μ for these slurries are listed in Table 9. It was further indicated that for the CWM made from the -325 mesh coal particles, the viscosity/shear-rate curves tended to the high-shear Newtonian limits η_∞ in Table 10. Correlations with concentration of these Newtonian viscosities of CWM were attempted using the following relative viscosity-solids volume fraction relations:

$$\eta_r=\left(1-\frac{\phi}{\phi_m}\right)^{-a} \quad (45)$$

$$\eta_r=\left(1-\frac{\phi}{\lambda}\right)^{-2} \quad (46)$$

Table 9. Reduced Viscosity-Concentration Dependence of CWM

Coal Sample (mesh)	$\bar{d}$ (μm)	ϕ_m (v/v)	λ Eq. 46	ϕ (v/v)	Reduced viscosity, η_r Expt.	Eq. 45*	Eq. 46	Eq. 47**
120/170	99.6	0.538	0.528	0.427	29.7	27.2	27.1	31.3
				0.471	70.9	78.4	84.5	63.2
170/230	73.2	0.531	0.519	0.390	17.1	16.7	17.2	22.1
				0.427	35.8	31.9	31.7	34.5
				0.476	94.0	123.4	143.8	84.3
230/325	50.9	0.516	0.501	0.379	20.0	17.3	16.8	22.6
				0.432	57.5	49.4	53.3	46.2
				0.469	110.3	172.0	240.9	104.7
-325	5.7	0.628	0.607	0.468	19.1†	20.2	19.2	25.2
				0.494	34.8	29.9	29.0	33.1
				0.563	128.1	146.6	193.6	93.0

* Coefficient a calculated from Eq. 48.
** Coefficient b calculated from Eq. 49.
† For the -325 mesh slurries $\eta_r=\eta_\infty/\eta_s$.

Table 10. Rheological Parameters for −325 Mesh CWM

				Equation 30		Equation 31	
ω (w/w)	ϕ (v/v)	η_∞ (poise)	τ_o ($g \cdot cm^{-1} \cdot s^{-2}$)	τ_b ($g \cdot cm^{-1} \cdot s^{-2}$)	η_b (poise)	τ_c ($g \cdot cm^{-1} \cdot s^{-2}$)	η_c (poise)
0.542	0.468	0.17	19.6	25.0	0.17	6.6	0.14
0.568	0.494	0.31	43.0	38.2	0.33	8.8	0.27
0.635	0.563	1.14	257.0	177.0	1.26	48.0	1.02

$$\eta_r = \left[1 - \left(\frac{\phi}{\phi_m}\right)^{1/3}\right]^{-b} \tag{47}$$

in which $\eta_r = \mu/\eta_s$ or η_∞/η_s is the relative viscosity, that is, the ratio of the viscosity of the slurry to that of the suspending medium, and a, b, and λ, which are positive, are model parameters. Aside from Eqs. 45-47, we tried the Frankel and Acrivos (1967) theory for the zero-shear viscosity of highly concentrated suspensions, Eq. 28 and the related expression of Sengun and Probstein (1989) for the infinite-shear viscosity. It was found that Frankel and Acrivos's equation underestimates the relative viscosity by a significant amount (by a factor in excess of from 2 to 5) and that Sengun and Probstein's expression predicts even lower values, as it must, since it pertains to the lower of the two Newtonian limits—the high-shear limit.

Comparisons between experimental relative viscosities and those predicted using Eqs. 45-47 are given in Table 9. The coefficients a and b are correlated with mean particle size using the approximate relations:

$$a = 2.206 - 1.119 \times 10^{-3}\bar{d} \tag{48}$$

$$b = 1.365 - 4.361 \times 10^{-4}\bar{d} \tag{49}$$

in which $\bar{d}$ is the number-mean particle diameter in μm. For our test slurries the coefficient a in Eq. 45 ranged from 2.087 and 2.200. These values are close to the exponent 2.0 in Eq. 46. Accordingly, one might expect Eqs. 45 and 46 to give similar prediction. The calculated values of the model parameter λ in Table 9 do follow closely the measured values of ϕ_m. From dilute limit expansions of Eqs. 45 and 47, it is evident that the magnitudes of (a/ϕ_m) and $(b/\phi_m{}^{1/3})$ provide measures of the relative degree of nonlinear (concentrated) behavior for any given solids loading. Furthermore, they are directly proportional to the rate of change of relative viscosity with solids concentration. It is clear, at least with narrowly sized particles, that for a given volume fraction of suspended solids, the smaller the particle size, the stronger the nonlinear behavior and the steeper the increase in viscosity with concentration. Equations 45 and 47 give the correct limiting values of the relative viscosity in the dilute and concentrated limits. Equation 46, however, need not give the correct high-concentration limit, since λ is a model parameter, not necessarily the value ϕ_m, but this equation has been found to be quite useful in correlating suspension viscosity data (Metzner, 1985).

Viscosity correlations of the sort given by Eqs. 45–49 may, like the yield stress correlations described before, be used as the bases for formulating CWM with desirable properties. This would entail preparing a particle size mix giving the desired limiting maximum solids loadings appropriate to the application, and combining this with the appropriate chemistry to give the desired rheological, and other characteristics and their rates of change with solids concentration. For coal-water fuel applications, for example, slurry viscosities under ordinary and high shear, and their rates of change with solids concentration, for loadings near the maximum packing limit, must be maintained at practically low levels. This can be accomplished by formulating CWF with high values of ϕ_m and low values of the parameters a and b, for example.

The shear-stress/shear-rate data for the −325 mesh CWM were fitted to the Bingham, the Casson and the Herschel-Bulkley models given by Eqs. 30–32. The least-squares-fitted model parameter values for the Bingham and Casson models are listed in Table 10. The Herschel-Bulkley model was found to result in unacceptably poor fit, giving deviations ranging from 60 to 90%. The yield stresses, τ_0, in Table 10 were obtained by interpolation of the experimental data from Table 8. The constants τ_b and τ_c, being model parameters, are not equal to these directly measured yield stresses, and indeed they are not even equal to each other. The Bingham plastic model does a reasonably good job of describing the shear-stress/shear-rate data for these slurries over the entire measured range, giving values with an absolute average per cent deviation of about 8.2 or less. The Casson model does a better job, resulting in deviations of less than about 6%. It is clear that both Bingham and Casson model parameters increase with increasing concentration.

Conclusions

This work is distinguished by the diversity of properties investigated for each coal-water slurry tested. These included the following: proximate and elemental analyses of the coal, and determination of its heating value, heat capacity and solid thermal conductivity; measurements of the particle size distributions and the maximum packing concentrations for each size fraction of coal particles; determination of the settling rates of all suspensions; direct measurements of suspension yield stresses as functions of solids concentration; and determination of the shear-stress/shear-rate dependences for different solids loadings over very broad ranges of shear. Aside from breadth of shear rate range, our shear-stress/shear-rate measurements are distinguished further by careful accounting for viscometer end and wall-slip effects. To our knowledge, there have been no published reports embodying a coherent array of diverse measurements of this breadth on the same test coal slurries and few works on coal slurry shear-stress/shear-rate dependence covering such a wide range of shear rates which are also unambiguously free of possible particle-viscometer interaction effects.

Narrow size fractions of coal particles, obtained by sieving, were used in this work to probe the effect of particle size on the behavior of coal-water mixtures. Because coal particles are irregularly shaped, however, there are intrinsic limits to the definition of particle size fraction. Nonetheless, detailed analyses of our particle size data in Table 4 suggest that the distributions for our three largest sized coal particles were fairly narrow as measured by the closeness of various particle size means and moments and by the values of the coefficients of variation. This is important, as it counts in sorting out the possible relative roles of dispersion of particle sizes or of complexity of shape on the observed behavior of our coal-water slurries. Other significant results and conclusions reached are as follows:

- Settling data for the three coarser, narrower-sized particles gave sediments that are relatively incompressible, consistent with unflocculated behavior. The settling velocity-concentration data are described very well by both the Richardson-Zaki form (Eq. 17) and the relation based on effective volume fraction (Eq. 33). Calculated values of the hindered settling index n in Eq. 17, however, are much larger than those for spherical particles, as expected for nonspherical particles (Chong et al., 1979). However, Stokes diameters d_{St} calculated from fitting Eq. 17 agree very closely with the measured mean (volume-equivalent) diameters, leading to inferred sphericities close to unity. This contradicts direct observation that our coal particles are irregularly shaped and therefore must have sphericities less than one. On the other hand, Eq. 33 describing the velocity-concentration data leads to Stokes diameters, which are smaller than the corresponding measured volume-equivalent particle diameters, and to calculated sphericities less than unity, as expected for nonspherical particles. When these different equivalent particle diameters are used to infer possible particle shape, we obtain ranges of shape consistent with and subsuming the directly observed shapes of our particles; platelike particles with relatively isodimensional, albeit irregularly-contoured, projections. Quantitative treatment of particle shape, similar, for example, to our analysis, is seldom attempted in studies involving multiparticle systems; shape is a silent variable.

- The shear-stress/shear-rate dependence of the slurries with the three coarser, narrower-sized particles was very nearly Newtonian. While affirming our previous conclusions (relative to settling) that the dispersion of sizes for these particles is narrow enough to have a relatively smaller effect, this finding is not inconsistent with the fact that the particles are irregularly shaped. Evidently, the low aspect ratios do not lead to shear-dependent effects, but do with increased concentration lead to marked viscosity enhancement and possibly anisotropic effects, which our experiments are not capable of ascertaining. This is an important finding for coal-water slurries, particularly since it is confirmed over such a broad range of shear rate and persists to such high solids loadings. By contrast and further confirming these conclusions for the smallest particles, the size distribution was clearly quite broad and the shear-stress/shear-rate dependence is found to be non-Newtonian.

- The yield stress-concentration correlations in Eqs. 37 and 38 and the simple viscosity-concentration correlations in Eqs. 45-47 incorporate the maximum packing solids concentration ϕ_m as a parameter. In our work, ϕ_m is determined independently by centrifugation. It is a geometric property of the particle size mix and not of suspension chemistry, and represents not only an upper limit to solids loading but also a limit near which slurry viscosity and yield stress approach unacceptably high values. However, the remaining parameters in these correlations are affected and can be controlled by slurry chemistry (Avramidis and Turian, 1991), and their values determine the rates of approach to high-yield and high-viscosity values as concentration approaches maximum packing. Within this context, such correlations can be used as the basis for formulating slurries with the desired yield-stress/viscosity-concentration dependences. Our measurements of ϕ_m confirm that narrow particle size distributions do not correspond to most efficient packing. Note that extrapolations to large yield stress value of detailed yield-stress/concentration data pertaining to different coal-water slurries in our laboratory result in ϕ_m values which are essentially the same as those determined independently by centrifugation (Fakhreddine, 1989).

- Our results are of general interest in understanding solid-liquid suspension behavior, and are specially useful in assessing the effects of particle size and solids loading on the relative stability to settling, and the flow behavior over broad ranges of shear of coal-water slurries. Coal analyses, the heating value, and the measured thermophysical properties pertaining to the test coal are included here because coal-water mixtures are used as a fuel.

Acknowledgment

This work was supported by funds from the U.S. Department of Energy under grant no. DE-FG22-84PC70781, the State of Illinois Center for Research on Sulfur in Coal, and the National Science Foundation under grant no. CBTE 8111258. We also acknowledge with gratitude help from Dr. Anthony G. Fonseca of Conoco, who supplied us with the test coals.

Notation

d = particle diameter, μm
$\bar{d}$ = number-mean particle diameter (Table 1), μm
D = cylinder diameter in sedimentation, capillary-tube diameter in rheometry, cm
F_D = drag force, N
k = $1/K$; shape factor
K = d_D/d_V, ratio of particle drag to volume diameter; shape factor
$\tilde{K}$ = consistency index in power-law model, Eq. 29, $g \cdot cm^{-1} \cdot s^{n-2}$
L = length of capillary tube, cm
n = hindered-settling concentration coefficients, Eq. 17
$\tilde{n}$ = flow behavior index in power-law model, Eq. 29
n_i = number of particles with diameter d_i
Re = $dv\rho/\mu$, particle Reynolds number
U = sedimentation velocity, $cm \cdot s^{-1}$
v = single-particle velocity, $cm \cdot s^{-1}$
w_i = mass of particles with diameter d_i

Greek letters

α_V = particle-volume shape factor ($= \pi/6$ for spheres)
$\dot{\gamma}$ = shear rate, s^{-1}
η = effective viscosity, P
κ = ratio of effective volume fraction of solids, including entrained liquid, to volume fraction of solids, Eq. 33
μ = Newtonian viscosity, P
ρ = density of liquid, g/cm^3
σ = standard deviation, Eqs. 8 and 9
τ = shear stress, $dyne \cdot cm^{-2}$
τ_0 = yield stress, $dyne \cdot cm^{-2}$
ϕ = volume fraction of solids
ϕ_m = maximum packing volume fraction of solids

χ = ϕ/ϕ_m
ψ = sphericity, Eq. 6
ω = weight fraction of solids

Literature Cited

Allendorfer, R. K., "Stability and Rheology of Size-Fractionated Coal-Water Mixtures," MS Thesis, Univ. of Illinois at Chicago (1990).

Alessandrini, A., I. Kikic, and R. Lapasin, "Rheology of Coal Suspensions," *Rheol. Acta*, **22**, 500 (1983).

Allen, T., *Particle Size Measurement*, 2nd ed., Chapman and Hall, London (1975).

Attal, J. F., "Characterization, Stability and Rheology of Coal-Water Mixtures," MS Thesis, Univ. of Illinois at Chicago (1989).

Avramidis, K. S., and R. M. Turian, "Yield Stress of Laterite Suspensions," *J. Colloid Interf. Sci.*, **143**, 54 (1991).

Barnea, E., and J. Mizrahi, "A Generalized Approach to the Fluid Dynamics of Particulate Systems: I. General Correlation for the Fluidization and Sedimentation in Solid Multiparticle Systems," *Chem. Eng. J.*, **5**, 171 (1973).

Becker, H. A., "The Effects of Shape and Reynolds Number on Drag in the Motion of a Freely Oriented Body in an Infinite Fluid," *Can. J. Chem. Eng.*, **37**, 85 (1959).

Bird, R. B., G. C. Dai, and B. J. Yarusso, "The Rheology and Flow of Viscoplastic Materials," *Revs. in Chem. Eng.*, **1**, 1 (1982).

Chester, W., and D. R. Breach, "On the Flow Past a Sphere at Low Reynolds Number," *J. Fluid Mech.*, **37**, 751 (1969).

Chong, Y. B., D. A. Ratkowsky, and N. Epstein, "Effect of Particle Shape on Hindered Settling in Creeping Flow," *Powder Tech.*, **23**, 55 (1979).

Christiansen, E. B., and D. H. Barker, "The Effect of Shape and Density on the Free Settling of Particles at High Reynolds Numbers," *AIChE J.*, **11**, 145 (1965).

Clarke, B., "Rheology of Coarse Settling Suspensions," *Trans. Instn. Chem. Engrs.*, **45**, 251 (1967).

Dzuy, Q. N., and D. V. Boger, "Direct Yield Stress Measurement with the Vane Method," *J. Rheol.*, **29**, 335 (1985).

Engez, S. M., "An Extension of the Study of Boundary Influence on the Fall Velocity of Spheres," MS Thesis, Univ. of Iowa, Iowa City (1948).

Fakhreddine, M. K., "The Yield Stress-Solids Concentration Dependence of Coal-Water Suspensions," MS Thesis, Univ. of Illinois at Chicago (1989).

Faxen, H., "Die Bewegung einer starren Kugel langs der Achse eines mit zahler Flussigkeit gefullten Rohres," *Arkiv For Matematik, Astronomi Och Fysik*, **17**, 1 (1922-23).

Fidleris, V., "The Fall of Spheres through Model Suspensions," PhD Thesis, Univ. of Nottingham, UK (1958).

Frankel, N. A., and A. Acrivos, "On the Viscosity of a Concentrated Suspension of Solid Spheres," *Chem. Eng. Sci.*, **22**, 847 (1967).

Garside, J., and M. R. Al-Dibouni, "Velocity-Voidage Relationships for Fluidization and Sedimentation in Solid-Liquid Systems," *Ind. Eng. Chem., Process Des. Dev.*, **16**, 206 (1977).

Greenstein, T., and J. Happel, "Theoretical Study of the Slow Motion of a Sphere and a Fluid in a Cylindrical Tube," *J. Fluid Mech.*, **34**, 705 (1968).

Haberman, W. L., "Wall Effect for Rigid and Fluid Spheres in Slow Motion," *Int. Cong. Appl. Mech., Brussels*, **3**, 210 (1956).

Happel, J., and H. Brenner, *Low Reynolds Number Hydrodynamics*, Prentice-Hall, Englewood Cliffs, NJ (1965).

Heiss, J. F., and J. Coull, "The Effect of Orientation and Shape on the Settling Velocity of Non-Isometric Particles in a Viscous Medium," *Chem. Eng. Prog.*, **48**, 133 (1952).

Hottovy, J. D., and N. D. Sylvester, "Drag Coefficients for Irregularly Shaped Particles," *Ind. Eng. Chem., Process Des. Dev.*, **18**, 433 (1979).

Hsu, F. L., R. M. Turian, and T. Z. Ma, "Flow of Noncolloidal Slurries in Pipelines," *AIChE J.*, **35**, 429 (1989).

Isaacs, J. L., and G. Thodos, "The Free Settling of Solid Cylindrical Particles in the Turbulent Regime," *Can. J. Chem. Eng.*, **45**, 150 (1967).

Jeffery, G. B., "The Motion of Ellipsoidal Particles Immersed in a Viscous Fluid," *Proc. Roy. Soc.*, London, **A102**, 161 (1922).

Jeffrey, D. J., and A. Acrivos, "The Rheological Properties of Suspensions of Rigid Particles," *AIChE J.*, **22**, 417 (1976).

Jinescu, V. V., "The Rheology of Suspensions," *Int. Chem. Eng.*, **14**, 397 (1974).

Lee, H. M., "A Modification of Stokes' Law to Account for Boundary Influence," MS Thesis, Univ. of Iowa, Ames (1947).

Leong, Y. K., D. E. Creasy, D. V. Boger, and Q. D. Nguyen, "Rheology of Brown Coal-Water Suspensions," *Rheol. Acta*, **26**, 291 (1987).

Lin, C. J., J. H. Peery, and W. R. Schowalter, "Simple Shear Flow Round a Rigid Sphere: Inertial Effects and Suspension Rheology," *J. Fluid Mech.*, **44**, 1 (1970).

McCabe, W. L., J. C. Smith, and P. Harriott, *Unit Operations of Chemical Engineering*, 4th ed., McGraw-Hill, New York (1985).

McNown, J. S., and J. Malaika, "Effects of Particle Shape on Settling Velocity at Low Reynolds Numbers," *Trans. Amer. Geophys. Union*, **31**, 74 (1950).

McNown, J. S., and T. J. Newlin, "Drag of Spheres within Cylindrical Boundaries," *Proc. U. S. Cong. Appl. Mech.*, Chicago, 801 (1951).

McNown, J. S., H. M. Lee, M. B. McPherson, and S. M. Engez, "Influence of Boundary Proximity on the Drag of Spheres," *Proc. Int. Cong. Appl. Mech.*, London, 17 (1948).

Metzner, A. B., "Rheology of Suspensions in Polymeric Liquids," *J. Rheol.*, **29**, 739 (1985).

Michaels, A. S., and J. C. Bolger, "Settling Rates and Sediment Volumes of Flocculated Kaolin Suspensions," *I & E C Fund.*, **1**, 24 (1962).

Nguyen, D. Q., and D. V. Boger, "Yield Stress Measurements for Concentrated Suspensions," *J. Rheol.*, **27**, 321 (1983).

Oseen, C. W., "über die Stokes'sche Formel und über eine verwandte Aufgabe in der Hydrodynamik," *Arkiv for Matematik, Astronomi Och Fysik*, **6**(29), 1 (1910).

Pettyjohn, E. S., and E. B. Christiansen, "Effect of Particle Shape on Free Settling Rates of Isometric Particles," *Chem. Eng. Prog.*, **44**, 157 (1948).

Pokrovskii, V. N., "Rheology of Disperse Systems and Polymers. Motion of Ellipsoids in Flow," *Colloid J. USSR*, **29**(4), 428 (1967).

Proudman, I., and J. R. A. Pearson, "Expansions at Small Reynolds Numbers for the Flow Past a Sphere and a Circular Cylinder," *J. Fluid Mech.*, **2**, 237 (1957).

Richardson, J. F., and W. N. Zaki, "Sedimentation and Fluidization: I," *Trans. Instn. Chem. Engrs.*, **32**, 35 (1954).

Rutgers, R., "Relative Viscosity of Suspensions of Rigid Spheres in Newtonian Liquids," *Rheol. Acta*, **2**, 202 (1962a); "Relative Viscosity and Concentration," *ibid.*, **2**, 305 (1962b); "Correction," *ibid.*, **3**, 118 (1963).

Selim, M. S., A. C. Kothari, and R. M. Turian, "Sedimentation of Multisized Particles," *AIChE J.*, **29**, 1029 (1983).

Sengun, M. Z., and R. F. Probstein, "High-Shear-Limit Viscosity and the Maximum Packing Fraction in Concentrated Monomodal Suspensions," *PhysicoChem. Hydrody.*, **11**, 229 (1989).

Stokes, G. G., "On the Effect of Internal Friction of Fluids on the Motion of Pendulums," *Trans. Camb. Philos. Soc.*, **9**, 8 (1861).

Steinour, J. H., "Rate of Sedimentation," *Ind. Eng. Chem.*, **36**, 618 (1944).

Thomas, D. G., "Transport Characteristics of Suspensions: VIII. a Note on the Viscosity of Newtonian Suspensions of Uniform Spherical Particles," *J. Colloid Sci.*, **20**, 267 (1965).

Tsai, S. C., and E. W. Knell, "Viscometry and Rheology of Coal-Water Slurry," *Fuel*, **65**, 566 (1986).

Whitehead, A. N., "On the Motion of Viscous Incompressible Fluids," *Quart. J. Math.*, **23**, 78 (1889).

Woeskobenko, F., S. R. Simeon, and D. E. Creasy, "Rheology of Victorian Brown Coal Slurries: 1. Raw Coal-Water," *Fuel*, **66**, 1299 (1987).

Manuscript received Sept. 9, 1991, and revision received Apr. 21, 1992.